OFFSHORE OIL SLICK DETECTION
WITH
REMOTE SENSING TECHNIQUES

A THESIS SUBMITTED TO
THE GRADUATE SCHOOL OF NATURAL AND APPLIED SCIENCES
OF
MIDDLE EAST TECHNICAL UNIVERSITY

BY

SERTAÇ AKAR

IN PARTIAL FULFILLMENT OF THE REQUIREMENTS
FOR
THE DEGREE OF MASTER OF SCIENCE
IN
GEOLOGICAL ENGINEERING

SEPTEMBER 2007

Approval of the Thesis:

OFFSHORE OIL SLICK DETECTION WITH REMOTE SENSING TECHNIQUES

submitted by **SERTAÇ AKAR** in partial fulfillment of the requirements for the degree of **Master of Science in Geological Engineering Department, Middle East Technical University** by,

Prof. Dr. Canan ÖZGEN
Dean, Graduate School of **Natural and Applied Sciences** _____

Prof. Dr. Vedat DOYURAN
Head of Department, **Geological Engineering Dept.** _____

Assoc. Prof. Dr. M. Lütfi SÜZEN
Supervisor, **Geological Engineering Dept., METU** _____

Assoc. Prof. Dr. Nuretdin KAYMAKCI
Co-Supervisor, **Geological Engineering Dept., METU** _____

Examining Committee Members

Prof. Dr. Nurkan KARAHANOĞLU
Geological Engineering Dept., METU _____

Assoc. Prof. Dr. M. Lütfi SÜZEN
Geological Engineering Dept., METU _____

Assoc. Prof. Dr. Nuretdin KAYMAKCI
Geological Engineering Dept., METU _____

Assoc. Prof. Dr. Bora ROJAY
Geological Engineering Dept., METU _____

Ali DEMİRER
Turkish Petroleum Company, T.P.A.O. _____

Date: 07.09.2007

I hereby declare that all information in this document has been obtained and presented in accordance with academic rules and ethical conduct. I also declare that, as required by these rules and conduct, I have fully cited and referenced all material and results that are not original to this work.

Name, Last name : Sertaç AKAR

Signature :

ABSTRACT

**OFFSHORE OIL SLICK DETECTION
WITH
REMOTE SENSING TECHNIQUES**

AKAR, Sertaç

M.Sc., Department of Geological Engineering

Supervisor: Assoc. Prof. Dr. M. Lütfi SÜZEN

Co-Supervisor: Assoc. Prof. Dr. Nuretdin KAYMAKÇI

September 2007, 77 pages

The aim of this thesis is to develop a methodology for detection of naturally occurring offshore oil slicks originating from hydrocarbon seeps using satellite remote sensing techniques. In this scope, Synthetic Aperture Radar (SAR) imagery has been utilized. Case study area was Andrusov High in the Central Black Sea. Hydrocarbon seepage from tectonic or stratigraphic origin at the sea floor causes oily gas plumes to rise up to the sea surface. They form thin oil films on the sea surface called oil slicks. Presence of seeps and surface oil slicks for the offshore basins is a trace of depleted oil traps. Spatial distribution of oil slicks is closely related to sea waves, dominant wind patterns and weathering factors. Even though, there are oil slick detection techniques available with optical remote sensing, laser fluorosensors, and hyperspectral remote sensing, the most efficient results can be obtained from active microwave sensors like synthetic aperture radar (SAR). SAR sensors simply measure the backscattered radiation from the surface and show the roughness of the terrain. Oil slicks dampen the sea waves creating dark patches in the SAR image. In this context an adapted

methodology has been proposed, including three levels namely; visual inspection, image filtering and object based fuzzy classification. With visual inspection, targets have been identified and subset scenes have been created. Subset scenes have been categorized into 3 cases based on contrast difference of dark spots to the surroundings. Then object based classification has been utilized with the fuzzy membership functions defined by extracted features of layer values, shape and texture from segmented and filtered SAR subsets. As a result, oil slicks have been discriminated from look-alikes which are the phenomena resembling oil slicks. The overall classification accuracy obtained by averaging three different cases is 83 % for oil slicks and 77 % for look-alikes. The results of this study can considered to be a preliminary work and supplementary information for determining the best operational procedure of offshore hydrocarbon exploration.

Keywords: Remote Sensing, Synthetic Aperture Radar (SAR), Offshore Petroleum Exploration, Black Sea, Oil Slick, Hydrocarbon Seepage

ÖZ

UZAKTAN ALGILAMA TEKNİKLERİ İLE DENİZEL PETROL SIZINTILARININ TESPİTİ

AKAR, Sertaç

Yüksek Lisans, Jeoloji Mühendisliği Bölümü

Tez Yöneticisi: Doç. Dr. M. Lütfi SÜZEN

Ortak Tez Yöneticisi: Doç. Dr. Nuretdin KAYMAKÇI

Eylül 2007, 77 sayfa

Bu tez, doğal olarak oluşan denizel petrol sızıntılarının uydu uzaktan algılama teknikleri ile belirlenmesini için bir yöntem geliştirmeyi amaçlamaktadır. Bu kapsamda, Yapay Boşluklu Radar (SAR) görüntüleme sistemi kullanılmıştır. Çalışma alanı olarak Orta Karadeniz'deki Andrusov yükseltisi seçilmiştir. Deniz tabanındaki tektonik yada stratigrafik kökenli hidrokarbon sızıntıları, petrol ve gaz kabarcıklarının deniz yüzeyine çıkmasına sebep olurlar. Burada yüzey petrol tabakası olarak tanımlanan ince yağ tabaklarını oluştururlar. Yüzey petrol tabakalarının ve yer altı petrol sızıntılarını varlığı gönülmüş petrol kapanlarının varlığına işarettir. Yüzey petrol tabakalarının mekansal dağılımı deniz dalgaları, baskın rüzgar yönü ve yüzeysel aşındırmalarla yakında ilişkilidir. Bu oluşumların tespitinde optik, lazer florsan ve hyperspectral gibi çeşitli uzaktan algılama yöntemleri olmasına rağmen en iyi etkin sonuçlar SAR gibi aktif mikrodalga algılayıcılarıyla elde edilmektedir. SAR algılayıcıları yüzey pürüzlülüğüne bağlı

olarak yansıyan radyasyonu ölçerler. Yüzey petrol tabakaları deniz dalgalarını sönümlendirerek SAR görüntüsü üzerinde koyu alanlar yaratırlar. Bu içerikte, görsel tarama, görüntü filtreleme ve nesneye dayalı bulutsu sınıflandırmayı içeren 3 seviyeli uyarlanmış bir yöntem önerilmiştir. Görsel tarama ile hedef alanlar belirlenmiş ve altküme görüntüler oluşturulmuştur. Daha sonra bu altküme görüntüler koyu alanların çevreleriyle olan zıtlık seviyelerine göre 3 kategori altında gruplanmıştır. Neneye dayalı sınıflandırma parazit temizleyici filtreleme ve morfolojik filtreleme yapılarak elde edilen altküme görülülerine kesimleme uygulanması sonucu oluşan vektörsel nesnelerin katman, şekil ve doku özellikleriyle tanımlanan bulutsu üyelik fonksiyonları ile yapılmıştır. Sonuç olarak yüzey petrol tabakaları "look-alike" olarak tanımlanan benzerlerinden ayrıştırılmıştır. Sınıflandırmanın farklı kategoriler için genel doğruluğu petrol tabakaları için % 83, bezer oluşumlar için ise % 77 olarak hesaplanmıştır. Bu çalışmanın sonuçları, denizel petrol araştırmalarının düzenlenmesinde destekleyici bir ön çalışma olarak değer kazanmaktadır.

Keywords: Uzaktan Algılama, Yapay Boşluklu Radar (SAR), Denizel Petrol Araştırması, Karadeniz, Yüzey Petrol Tabakası, Yeraltı Hidrokarbon Sızıntısı

To My Parents and My Sister Simay

ACKNOWLEDGEMENTS

It is an honor for me to express my admiration and esteem to my supervisor Assoc. Prof. Lütfi Süzen for his understanding, continuous support, unlimited trust, supervision and patience throughout the study. His intervention on crucial points rendered the thesis a worthwhile work.

I am grateful to Assoc. Prof. Dr. Nuretdin Kaymakçı for his continuous support, trust, and encouragement which enabled me to visualize the related concepts in different aspect and improve myself in a positive attitude.

I would like to thank to my instructors Dr. Valentyn Tolpekin and Dr. Norman Kerle from International Institute for Geo-information Science and Earth Observation (ITC) Enschede, Holland for their support on image processing and classification techniques, and help for the usage of eCognition Software.

I would also like thank to my colleagues Nesrin Tüfekçi, Başak Sener, Pınar Kaymakçı and Çağıl Kolat form GIS and Remote Sensing Laboratory for their unlimited patience and support for TNTmips software usage, remote sensing concepts and methods throughout every stages of my work.

I would especially like to thank to Turkish Petroleum Company (T.P.A.O.) for provision of ENVISAT-ASAR images.

I also would like to thank to Ali Demirer, and Serhan Çopur from T.P.A.O. for giving me the chance to be involved in the crew of "Piri Reis" offshore petroleum exploration cruise at Black Sea.

Finally, I would like to express my special thanks to my parents and my sister Simay who always support and motivate me and who truly merit the dedication of this thesis.

TABLE OF CONTENTS

CHAPTERS

LIST OF TABLES

TABLE

LIST OF FIGURES

FIGURE

CHAPTER 1

INTRODUCTION

The growing demand for energy and raw materials has enlarged the gap between available resources and future needs. The augmentation in the energy demand force oil companies to find more fields. As a consequence, oil companies throughout the world have to direct their exploration activities towards remote areas, rough seas, deep oceans and the Polar Regions. Today, feasibility studies for oil exploration and exploitation are based on wide-ranging information, concerning not only geology and related disciplines, but also, increasingly, geophysics, oceanography and statistics on sea-state and wind conditions. Here is where space imagery and remote sensing can play a crucial role.

There are many remote sensing applications for onshore oil fields based rock soil and mineral alterations (Van der Meer et al., 2002; Almeida-Filho et al., 1999) and for the offshore fields related to oil slicks on the sea surface (O'Brein et al. 2005; Almeida-Filho et al., 2004; Struckmeyer et al., 2002). These oil slicks can be detected with optical and microwave remote sensing techniques (Brekke and Solberg, 2005; Fingas and Brown 1999). Microwave remote, sensing especially synthetic aperture radar (SAR) is considered to be the most common and effective way (Solberg et al., 2007; Marghany, 2001; Fiscella et al. 2000; Espedal, 1999).

Oily gas plumes escaping from subsurface structures rise to the sea surface without a little dispersion of internal water currents. When they reach to sea surface they aggregate to form thin film called oil slicks. In fact, oil slicks are on sea surface are from various sources such as; man made slicks from illegal discharges of ships (Lu, 2003) or by accidents, slicks originated from biological activities such as photo-oxidation processes or by planktons, and geological slicks originated from natural hydrocarbon seeps. Counting every kind of slicks, 10 percent of ocean surface is estimated to be covered by slicks (Girard-Ardhuin et al. 2003). The phenomenon in our

concern is the naturally occurring oil slicks from natural hydrocarbon seepages. Oil slicks on the sea surface are seen relatively often and commonly appearing in connection with wind patterns and atmospheric conditions.

Oil slick detection is one of the significant preliminary works for offshore petroleum exploration. However, it does not explain the whole petroleum system by itself. It should be combined with seismic interpretation, sample collection from sea bottom and geological survey. There are many examples of these kinds of studies all around the world and well-known ones are the Gulf of Mexico (Friedman et al., 2002), Santa Barbara Channel, California (Leifer et al., 2006) and Australian Shelf (O'Brein et al. 2005). One of the newly emerging research areas for the offshore petroleum exploration is the Black Sea. Black sea is very important for potential methane and hydrocarbon accumulations since drainage of many of the major rivers of Eurasia into the Black Sea has resulted in the accumulation of a very thick Neogene through Recent sedimentary section (Roberts, 1998). The phenomenon of hydrocarbon seeps in The Black Sea Basin has also been investigated by many researchers (Greinert et al., 2006; Ergün et al., 2002; Kruglyakova et al., 2002). In this study Black Sea has been selected as a case study for application of SAR remote sensing techniques for the oil slicks detection.

Remote sensing techniques for oil slick detection are not a new concept and have been used for some petroleum fields. Every wavelength of electromagnetic spectrum is susceptible to different characteristic of oil on sea water (Fingas and Brown 1999). Different satellite sensors are available for data accusation from different electromagnetic wavelengths. They are both active, emitting and receiving its own electromagnetic pulse and passive sensors, receiving reflections from solar radiation. For instance, sensors obtaining data from visible and shortwave infrared wavelength susceptible to reflectance, thermal infrared wavelength is sensitive to thermal emmisivity, and microwave is susceptible to backscatter pulse.

Microwave backscatter data gives us information about the surface roughness. Oil slicks dampen the sea water and this dampening affect first examined and explained as a function of slick elasticity by Marangoni (1872) see Girard-Ardhuin et al. 2003. Consequently, oil slicks appear as dark areas in a SAR image. This primary information will be the basis of all image

processing and classification methods. Rather than oil slicks, there are some other natural phenomena that dampen the short sea waves and dark patches on the surface called look-alikes (Hovland et al.1994, Solberg et al. 1999).There are several methodologies developed for oil slick detection from SAR data. The techniques are different but main scope is to detect and classify dark patches based on some knowledge based decision parameters. Image filtering is compulsory for the preliminary stage of dark spot detection and there are various filtering algorithms for this purpose.

1.1. Hydrocarbon Seepage & Oil Slick

Hydrocarbon seepage is, the surface expression of a migration pathway, along which petroleum is currently flowing, driven by buoyancy from a sub-surface origin (Clarke & Cleverly, 1991). Hydrocarbon seepages are form either tectonic or stratigraphic origin (MacDonald, 2002). Hydrocarbons migrate rapidly through sediment column with little geochemical alteration. Microbial degradation of near surface oil greatly depletes the normal and branched alkenes in the oil and produces an end product of unresolved complex mixture of tars (MacDonald, 2002). However, most of the dispersion is not on the way to the sea surface but just after the oil and gas bubbles reaches the sea surface. Oil detection depends on the local weather conditions that determine its fate on the water's surface (Nirchio et al., 2005).

1.1.1. Significance of Seeps in Petroleum Exploration

Transpiration of oil and gas seeps is an essential piece of evidence that helps to narrow down a region for potential exploration for oil and gas accumulations. Basically, seeps demonstrate that a basin contains a generating source rock and therefore a viable petroleum reserve. Hydrocarbon seepage is widespread throughout the world; especially continental margins have the potential to provide a huge oil and natural gas resource. The presence of seepage, with sufficient amounts of hydrocarbon for detailed molecular characterization, can provide key petroleum systems information about source type and age, primary and secondary migration pathways, and level of organic maturity (Abrams, 2005).Seeps can be

observed both onshore and offshore. Offshore seeps are common in the sedimentary record and have characteristic morphological signatures such as pockmarks, piping and rills carbonate bodies in various shapes and settings.

It has been demonstrated by the oil companies' research, that over 75% of the world's oil generating basins contain surface seeps, the exceptions being those with unbroken regional evaporitic seals. Most seeps represent tiny but detectable volumes of oil and gas which are not significantly depleting the reservoir. Exceptions would be in some Recent onshore fold and thrust belts where accumulations have either been breached or redistributed to Tertiary traps and where the link between surface seeps and the leaking traps is more complex. Such geology, however, is rarely encountered in offshore basins so that problem does not arise.

1.1.2. Mechanisms and Sources of Hydrocarbon Seeps

Formation of hydrocarbon seeps at the seafloor can be due to various factors where the rate of migration is high (MacDonald, 2002). Empirical observations and computer simulations suggest that the mechanism for micro-seepage is a buoyancy-driven, continuous-phase gas flow through water-wet pores and fractures (Rollet et al. 2006). Generally seeps may result from fault systems, mud volcanoes, stratigraphic origin or combination of all (Figure 1.1). Evidence of hydrocarbon seeps is often associated with mud volcanoes or mud domes or pockmarks. Mud volcanoes are more common within active accretionary prisms or other compressional settings and pockmarks are common in various tectono-stratigraphic settings. (Rollet et al 2006). As an example of tectonically originated seepage can be given as Foz do Amazonas Basin, Brazil in Figure 1.2 (Almeida-Filho et al., 2004). The amount of seepage potentially is related to the pressure in oil and gas reservoirs, which in turn is related to hydrostatic pressure and changes in lithospheric stress. Hydrocarbon seepage can be classified into two major categories according to the scale. Macro-seeps are the visible presence of oil and gas seeping to the surface and micro-seepages are hydrocarbons seeping probably vertically or near-vertically from the reservoir to the surface (Van der Meer et al. 2002).

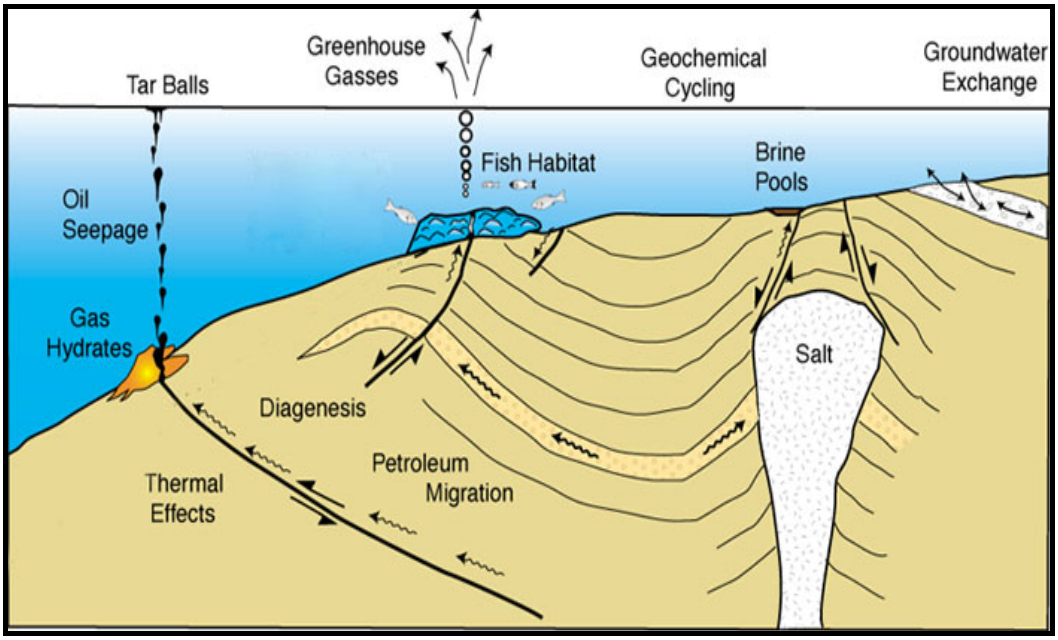

Figure 1.1: Schematic cross section of different seepage systems both tectonic and stratigraphic (Source: AAPG/American Association of Petroleum Geologists).

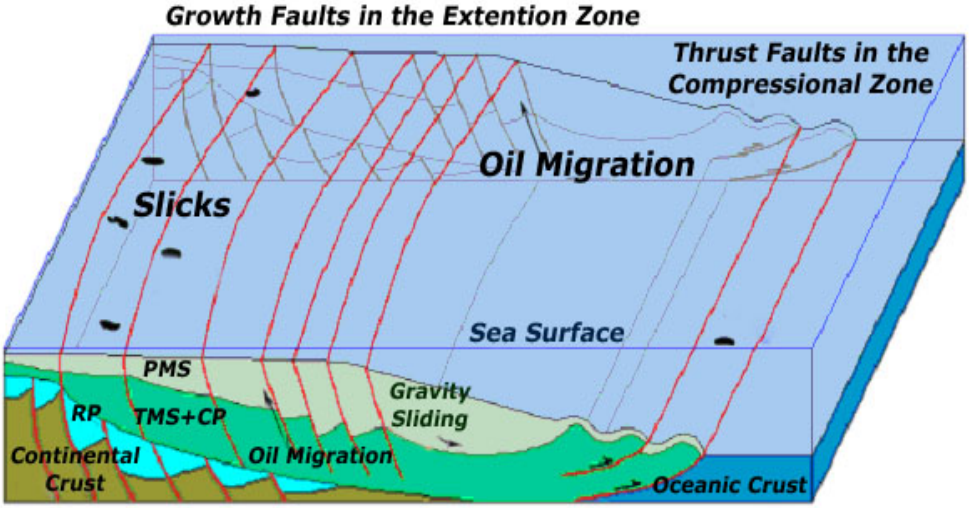

Figure 1.2: Gravity sliding tectonic model controlling the distribution of seepage slicks in the Foz do Amazonas Basin (RP= Rift Phase; TMS+CP= Transgressive Marine Sequence + Marine Carbonate Platform; PMS= Prograding Marine Sequence (Almeida-Filho et al., 2004)

Petroleum seepage system is composed of seepage type, seepage activity, migration focus and near surface seep disturbances (Abrams, 2005). Seepage type is related to scale whether it is micro or macro seep, seepage activity is related to continuity of the incoming flux, and migration focus is based on the seepage migration mechanisms (Abrams, 2005). Migration vertically through the strata is controlled by three seepage mechanisms which are effusion; due to the very large pressure differentiation that exists across a petroleum reservoir (see Abrams, 2005), diffusion; because of dissolved gases in vertically migrating waters that can be observed passing through seemingly impenetrable barriers (see Abrams, 2005), and vertical movement low molecular weight hydrocarbons dissolved in water through capping shales as a result of hydrodynamic or chemical potential drive (Van der Meer et al. 2002).

The seeping oil and gas are typically considered to rise rapidly to the surface and are often transported as thin slicks on the surface of gas bubbles (O'Brein et al., 2005). These bubbles have been shown to rise at speeds exceeding those of ocean currents and hence seepage slicks are typically developed initially on the sea's surface no further away from the seafloor seepage vent than a distance roughly equivalent to the water depth. The initial size of the bubble is determined by the size and shape of the active spot. The bubble upwelling flow and dissolved CH_4 concentration can affect bubble survival (MacDonald, 2002).

1.1.3. Formation of Oil Slicks

Offshore oil slicks are highly time depended structures and requires a detailed survey of comparison of individual seep activities over time. Some slicks are observed to be perennial since they are produced approximately in the same location in multiple images. This location is determined as producing a buffer zone to each individual slick. The weather conditions especially the wind speed and the wind direction causes this variation in the location of the oil slicks. Heavier (Low API) oils are the easiest to detect because they have longer residence times at the sea surface, whereas condensates and light oils evaporate much more rapidly (O'Brein et al., 2005).

Oil and Gas bubbles travel through the water column and at the sea surface, the gas bubble bursts and oil remains on the surface as a thin oil film. In calm sea conditions, these can often be viewed as beautiful, iridescent concentric shapes, typically 0.5 to 1 meter in diameter, known as 'oil pancakes' (Figure 1.3). The relation between the persistence of seepage and seafloor geology depends on the degree to which sediments and gas hydrate deposits will retard the escape of hydrocarbons. Gas hydrate deposits, particularly those that breach the sea floor exists at equilibrium between hydrate formation in the gas saturated pore volume of the shallow sub-bottom and hydrate dissociation at the water-hydrate interface. The deposits breach and vent where gas flux gas flux is vigorous (MacDonald, 2002)

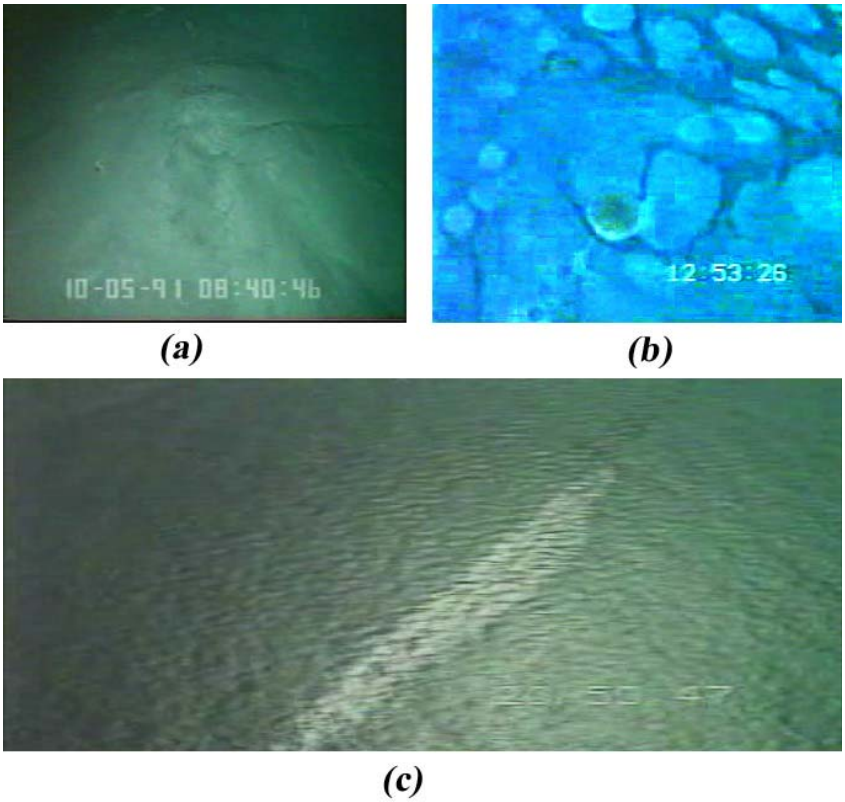

Figure 1.3: History of oil Slick Formation. (a) Hydrocarbon release from subsurface structures. (b) Oil and gas bubbles reaching to sea surface. (c) Oil bubbles aggregate to form a slick. (Source: European Space Agency)

1.1.4. Behavior of Oil Slicks at Sea Surface

Oil slicks on the sea surface undergo some physical and chemical changes affecting their distribution and temporal existence. The various processes of weathering are spreading, evaporation, dispersion, emulsification, dissolution, oxidation, sedimentation and biodegradation. The schematic representation of different types of weathering processes can be seen in Figure 1.4 and their impact on the slicks based on temporal concerns is represented in Figure 1.5.

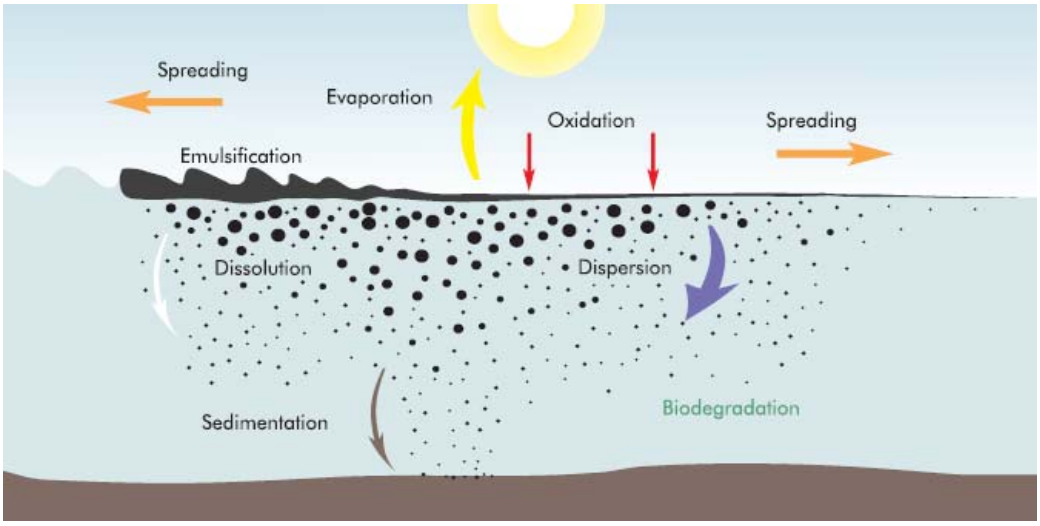

Figure 1.4: Weathering processes affecting oil slicks on sea surface (ITOPF, 2002).

1.1.4.1. Spreading

Spreading is the earliest stage of weathering after the formation of oil slick on the sea surface. Viscosity and amount of oil affect the rate of spreading. Low viscosity oils spread more quickly than those with a high viscosity. Few hours after, slicks starts to break up and form narrow bands parallel to the wind direction (Pellemans et al. 1995; Daling and StrØm, 1999). After that stage the spreading is controlled by winds, wave action and

water turbulence. Slicks can spread over several square kilometers in just a few hours and over several hundreds of square kilometers within a few days depending on the coming oil flux. For natural seeps the flux rate is not sufficient enough to spread greater distances and weathered by other factors before being spread (Pellemans et al. 1995).

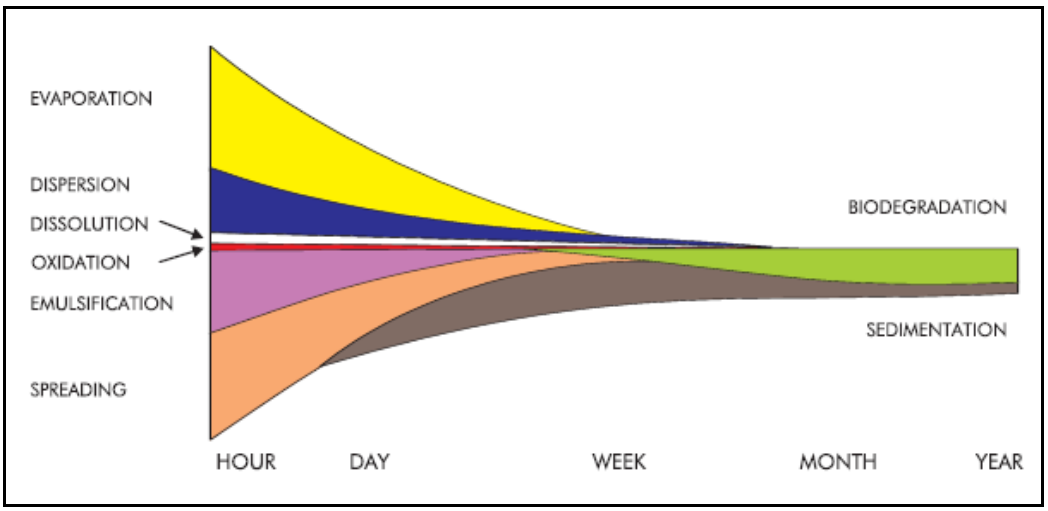

Figure 1.5: Effect of weathering processes with respect to time (ITOPF, 2002).

1.1.4.2. Evaporation

The rate of evaporation depends on volatility, ambient temperatures and wind speed (Nirchio et al., 2005). In general, oil components with a boiling point below 200°C will evaporate within a period of 24 hours in temperate conditions (Pellemans et al. 1995). The initial spreading rate of the oil also affects evaporation since increasing surface area will increase the rate of evaporation. Rough seas, high wind speeds like Black Sea and warm temperatures will also increase the rate of evaporation. In addition to this refined oil products may evaporate completely within few hours but extremely volatile oils undergo little evaporation (Pellemans et al. 1995, Daling and StrØm, 1999).

1.1.4.3. Dispersion

Slicks can be broken into droplets of different sizes partially or completely because of waves and turbulence at the sea surface. However, some smaller droplets may remain in suspension, while the larger ones rise back to the surface, where they either integrate with other droplets to reform a slick or spread out in a very thin film (Pellemans et al. 1995). Increment in surface area can trigger other weathering processes. Main factors in dispersion rate is the nature of the oil and the sea state, proceeding most rapidly with low viscosity oils in the presence of breaking waves (Pellemans et al. 1995).

1.1.4.4. Dissolution

The rate and extent of oil dissolution depends on composition, spreading, water temperature, turbulence and degree of dispersion (Pellemans et al. 1995; Daling and StrØm, 1999). The light oils and hydrocarbons or refined end products are slightly soluble in water but they disappear 10 to 1000 times more quickly by evaporation. However, heavy oils like crude oil are virtually insoluble in water. Also the most volatile and are lost very rapidly by evaporation, Concentrations of dissolved hydrocarbons in sea water thus rarely exceed 1 ppm and dissolution does not make a significant contribution to the weathering of oil on the sea surface (Pellemans et al. 1995).

1.1.4.5. Emulsification

In the seas with moderate to rough weather conditions, oils absorb water droplets in the form water-in-oil emulsions due to the turbulent action of waves on the sea surface. At wind speed of 7 - 10 knots oil emulsifies rapidly (Pellemans et al. 1995). Absorption of water usually results a color change in oil from black to brown orange or yellow. As the emulsion develops, the movement of the oil in the waves causes the droplets of water which have been taken up in the oil to become smaller making the emulsion more viscous. However, emulsions may separate out into oil and water when heated by the sunlight (Pellemans et al. 1995).

1.1.4.6. Oxidation

When hydrocarbons react with oxygen they may either lead to the formation of soluble products or persistent tars. Oxidation can occur at any time where the slick is present but mostly sunlight promotes it. When compared to other weathering processes it has very little effect. Even under intense sunlight, thin oil films break down only slowly, and usually less than 0.1% per day (Pellemans et al. 1995).

1.1.4.7. Sedimentation

Oils having specific gravities greater than sea water, which is 1.025, sink through the water column. Most crude and hydrocarbons have sufficiently low specific gravities which lead to float on sea surface. If dispersed oil droplets interact with and attach to more dense sediment or organic particles they become heavier and start to sink. It is not common to observe great amount of sedimentation in the offshore environment but the high energy environments like shallow waters, waters of river mouths, estuaries and beaches are very suitable (Pellemans et al. 1995).

1.1.4.8. Biodegradation

Sea water contains plenty of micro-organisms like bacteria, moulds, yeasts, fungi, unicellular algae and protozoa utilizing oil as a source of carbon. They are widely distributed all around the world's oceans but more abundant in polluted areas, high vessel traffic areas and areas of industrial discharges and untreated sewage and they can reproduce quickly when oil is present (Pellemans et al. 1995). Biodegradation occurs by acting of micro-organisms together or in succession depending on the specific group of hydrocarbon and controlled by oxygen and nutrients, principally compounds of nitrogen and phosphorus, and temperature (Pellemans et al. 1995).

1.2. Petroleum Geology of The Black Sea

The Black Sea is a semi-enclosed sea located between 40°55^{o} to 46°32^{o} N and 27°27^{o} to 41°32^{o} E, whose only connection to the worlds'

oceans is the narrow Bosporus Channel. Total area is 436,400 km^2 with maximum and average depths of 2200 m and 1240 m, respectively. The study area is just located at the center of the basin which is called Andrusov high separating the eastern and the western basins and covered by 4 sets of ENVISAT-ASAR images (Figure 1.6).

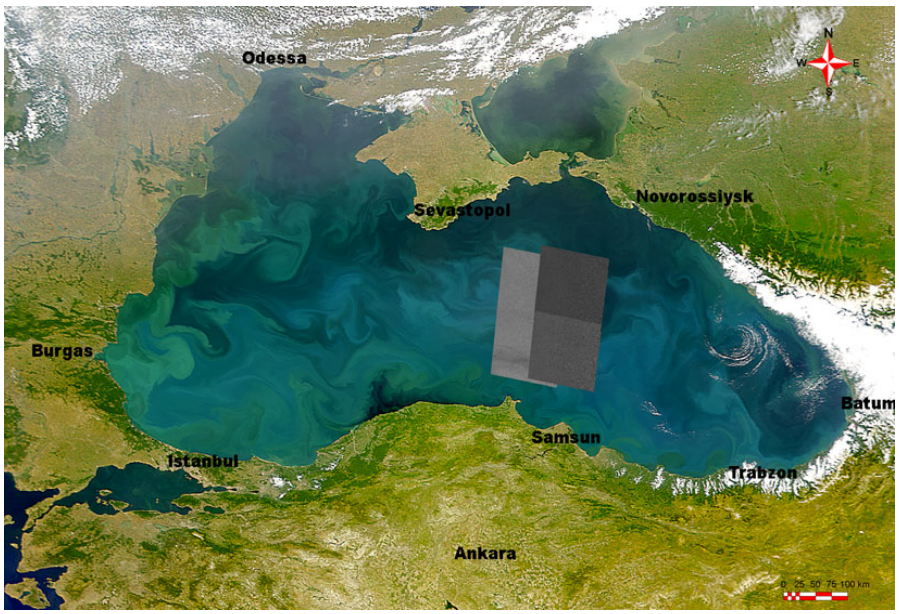

Figure 1.6: Location map of Black Sea Showing the Study Area with ENVISAT-ASAR images.

1.2.1. Regional & Structural Geology

The Black Sea is the world's largest anoxic marine basin which comprises two extensional basins separated by the Andrusov Ridge (Mazzini et al., 2004; Robinson et al., 1996; Okay et al., 1994). The two extensional basins are most probably at different ages. They combined at their late post-rift phases in the Pliocene, forming a single depocentre (Nikishin et al., 2003). Western Black Sea Basin is originated as a back-arc basin within complex folded chains of the Alpine system near southern margin of Eurasia,

which is inpresent-day Odessa shelf, above the northward subducting Tethys Ocean by tearing a Hercynian continental sliver (Okay et al., 1994). The Eastern Black Sea probably was opened by separation of the Mid-Black Sea High from the Shatsky Ridge during the Palaeocene to Eocene due to the counterclockwise rotation of an east Black Sea block around a rotation pole located north of the Crimea (Robinson et al., 1996; Okay et al., 1994). A general view of regional and structural geology can be found in Figure 1.7.

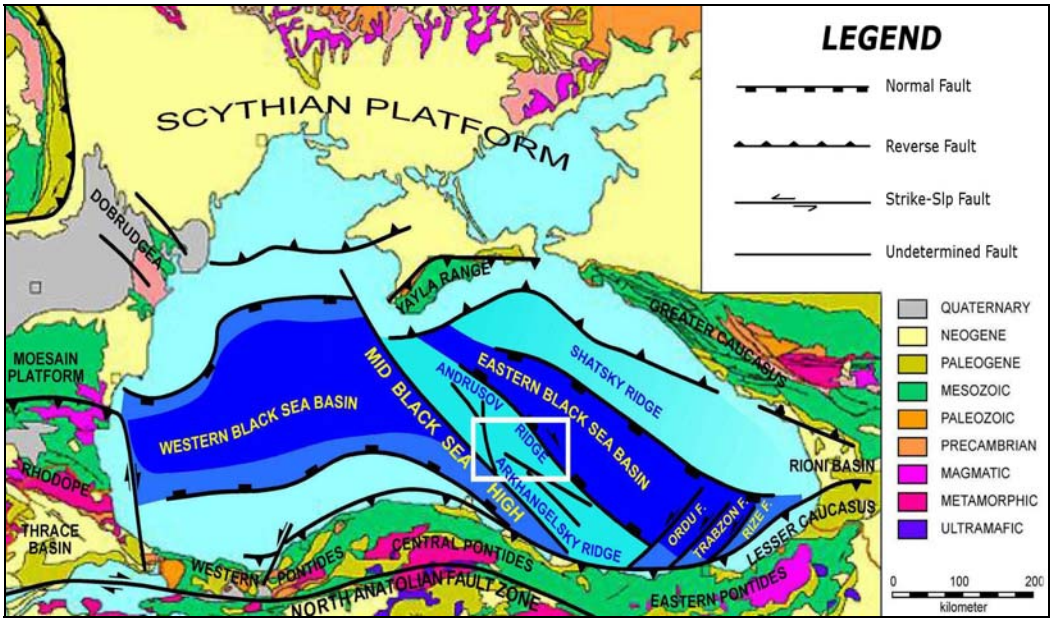

Figure 1.7: Regional Geology and tectonics of The Black Sea. (White rectangle roughly represents the study area) (modified from T.P.A.O., 1997)

1.2.2. Petroleum Potential

Recent studies in marine geology indicate that there is great hydrocarbon potential in the Black Sea. There are several fields for the oil and gas generation through out the basin. Compressional anticlines and extensional structures in Gulf of Odessa (Robinson et al. 1996), mud volcano area in the deep waters southeast of the Crimea Peninsula (Greinert et al.

2006), foreland basin extensional structures of Bulgarian waters and Romanian shelf (Robinson et al. 1996), Central Azov High around the Sea of Azov, Shatsky Ridge offshore Russia and Georgia, compressional structures off the northern Turkish coast (Ergün et al. 2002), The extensional fault blocks of the Andrusov Ridge are seen as having the best hydrocarbon potential (Robinson et al. 1996).

1.2.3. Petroleum System

During Jurassic and Cretaceous Andrusov Ridge was rifting Stage and in Tertiary whole Black Sea Basin was in compression leading extensional collapse and uplifting of Eastern Pontites. Geological and geophysical evaluations in the Eastern Black Sea Basin and Andrusov Ridge reveal that possible source rocks for the oil generation Eocene carbonates, and Oligocene-Miocene Maykop Formation and Aptian-Albian shales in Çağlayan Formation (Roberts, 1998; TPAO, 1997). Oil generation started 7 million years ago (Late Miocene) whereas gas generation in the deepest part started 1.6 million years ago; both oil and gas generations continue in the present time from 4000m thick Maykop section (TPAO, 1997). Reservoir rocks are namely, Oligocene-Lower Miocene sandstones inter-tonguing with source shales (Maykop Formation), Aptian-Albian Sandstones (Çağlayan Formation), Upper Jurrasic- Neocomian Limestones (İnaltı Formation), and Maastrichtian Carbonates (Alveren Formation) (TPAO, 1997). Deep marine pelagics and Miocene-Pliocene transgressive marine shale intervals can serve as seal for Mio-Pliocene reservoirs. Figure 1.8 represents the generalized columnar section of the "Turkish Eastern Black Sea" (TPAO, 1997).

1.2.4. Oil & Gas Seeps

The nature of hydrocarbons in the marine environment of the Black Sea is quite diverse including syngenetic biogenic gases, deep epigenetic gases, and technogenic hydrocarbon components (Kruglyakova et al. 2002). According to seismic and acoustic data, the signs of hydrate-bearing sediments have been detected on the continental slope in the West Black Sea Basin and in the East Black Sea Basin between the foot of the Caucasus slope (Russia) and the East Pontides (Turkey) (Kruglyakova et al., 2002).

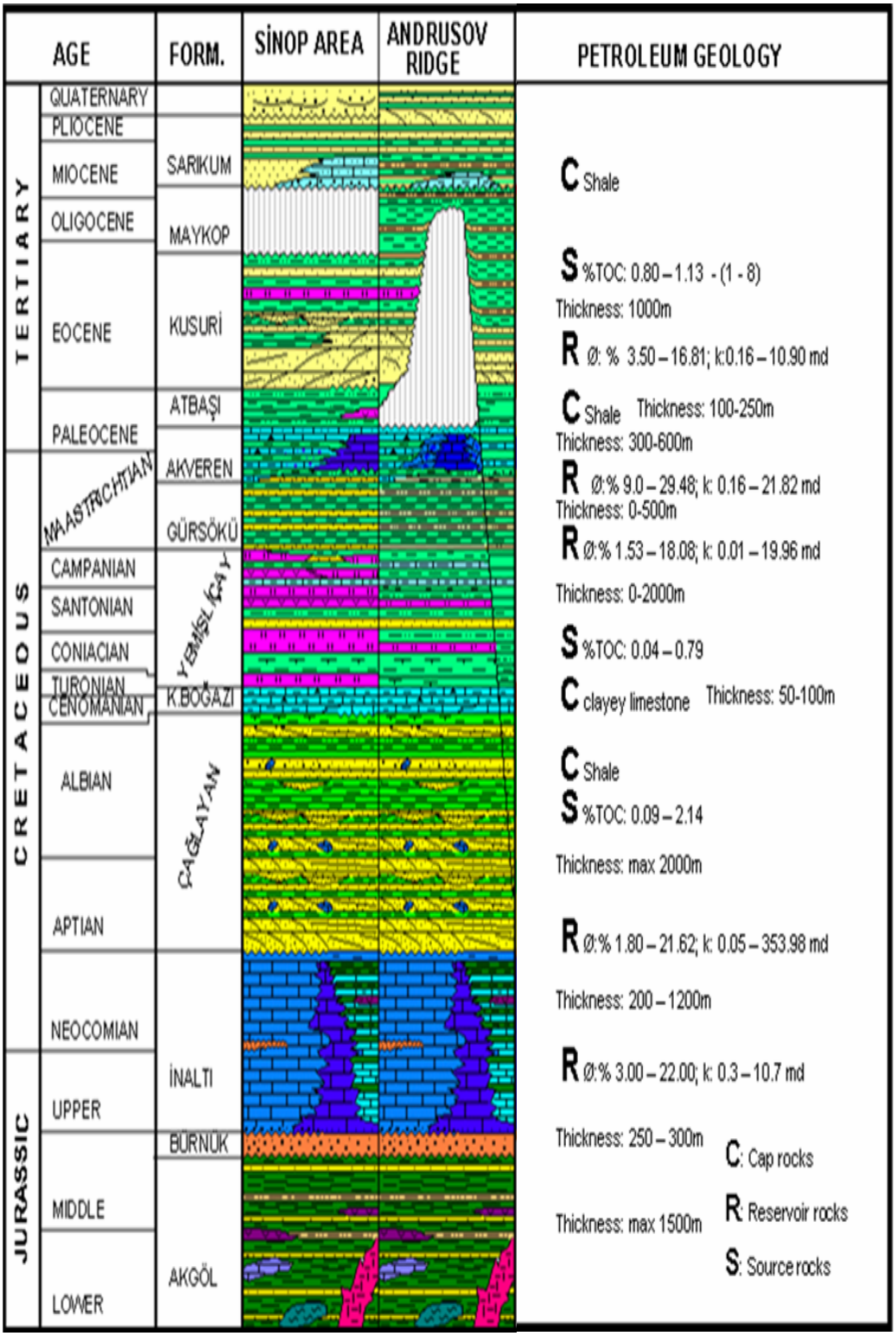

Figure 1.8: Generalized Columnar Section of Andrusov Ridge and Sinop Area (TPAO, 1997)

The Eastern Black Sea has extensive methane and methane hydrate accumulations, and structures related to gas plumes, gas-saturated sediments and pockmarks can be observed all around the Eastern Black Sea basin (Ergün et al. 2002). Strong scatter in the data indicates multiple source rocks of varying maturity onshore although the offshore Rize seep oils seem to have been sourced from an Eocene Maykopian source (Roberts, 1998). The Turkish Shelf of the Eastern Black Sea is characterized by intense gas masking, gas seepage and a mottled surface on the shallower part, while parallel beds with a rippled unconformable surface are found on the deeper part (Ergün et al.2002). There are pockmarks up to 50 m diameter and several meters deep which are related to local subsidence and faulting due to the escape of biogenic and hydrothermal gas.

1.2.5. Regional Factors

Atmospheric conditions show temporal and spatial variability in Black Sea. Vigorous mesoscale eddies, meanders and filaments have been revealed which pinch off coastal recirculation regions or Rim Current intrusions towards deep water (Staneva et al. 2001). General water circulation in the Black Sea consist of two cyclonic gyres that nearly split the basin area into two and a series of cyclonic and anti-cyclonic mesoscale eddies that appear to come from the larger-scale features (Bakan and Büyükgüngör, 2000). In a detailed manner, the number of major eddy currents in the Black Sea reaches up to 12 and their locations can be seen in Figure 1.9 (Staneva et al. 2001).

The most important factor on surface thin film spatial distribution and dispersion is the wind characteristics of the region. In The Black Sea Speed and Direction of wind and height of sea waves shows variation during the year. A detailed survey for wind and wave characteristics have been conducted around the Turkish coast of Black Sea including the 8 year data from 1991 to 1999 (see Özhan and Abdalla 2002). For an observation point close to our study area shown with a "black star" in Figure 1.9, rose diagrams for wind and sea wave direction (Figure 1.10), statistical evaluation of monthly wind speed variation (Figure 1.11), and the monthly sea wave height variation (Figure 1.12) has been represented.

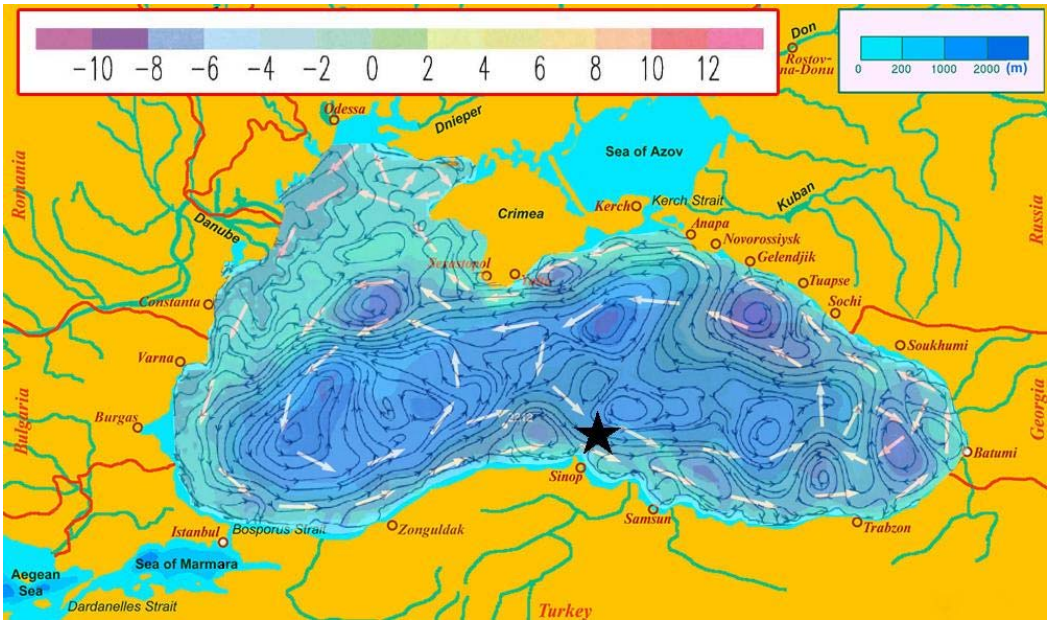

Figure1.9: The predominant semi-permanent elements of the general wave and wind circulation in the Black Sea (Modified from Steneva, 2001).

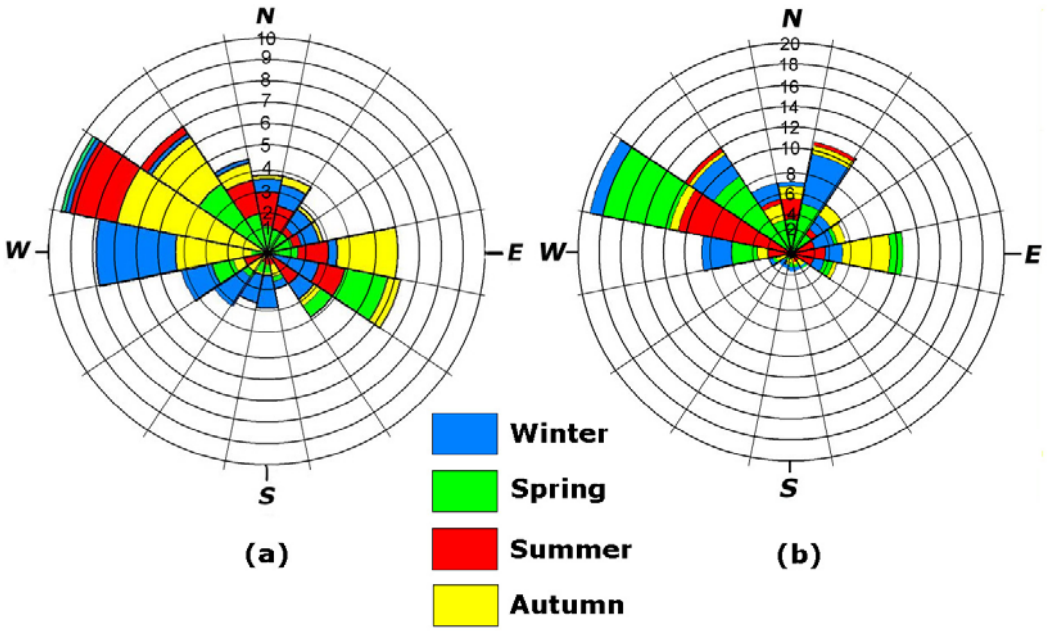

Figure 1.10: Rose Diagrams representing (a) dominant wind directions and (b) dominant wave directions in 4 different seasons around deep waters of Sinop (Data: Özhan and Abdalla 2002)

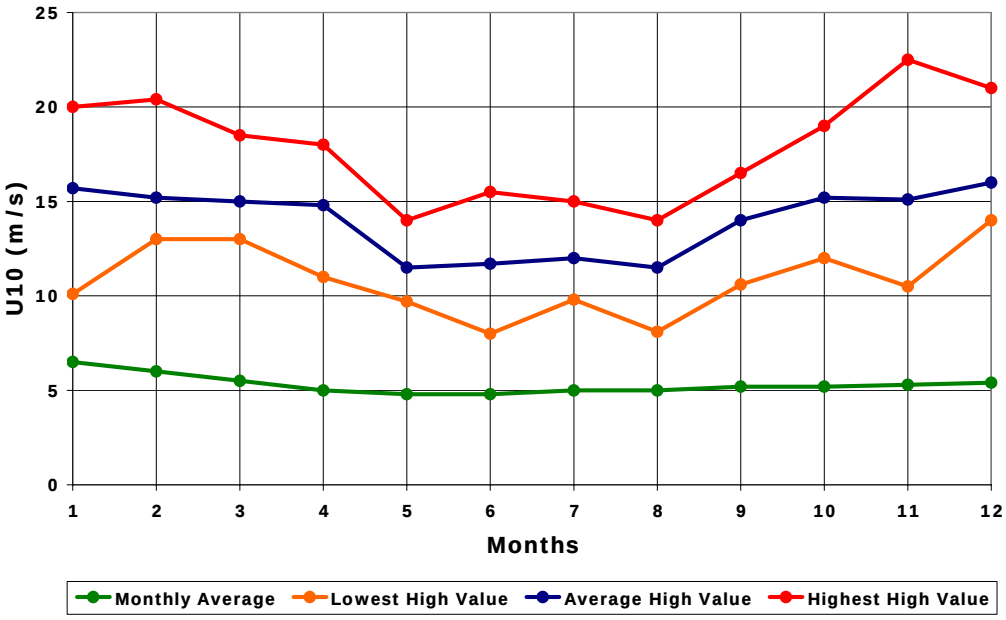

Figure 1.11: Monthly wind speed variation around deep waters of Sinop (Data: Özhan and Abdalla 2002)

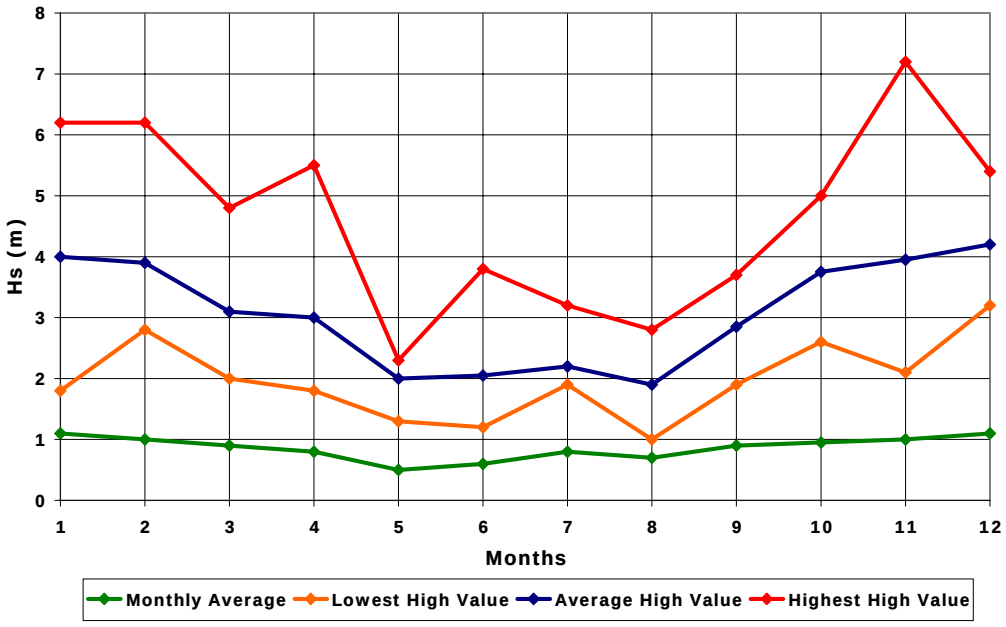

Figure 1.12: Monthly wave height variation around deep waters of Sinop (Data: Özhan and Abdalla 2002)

1.3. Oil Slick Remote Sensing Overview

There are different remote sensing applications for detection of offshore oil slicks. These include ultraviolet, visible, infrared and microwave wavelength regions of the electromagnetic spectrum. Oil slicks give different responses to radiation from different wavelengths. The main focus will be on the microwave remote sensing since the major goal of the research is utilization of Synthetic Aperture Radar (SAR).

1.3.1. Ultraviolet

UV technology can be used to detect oil spills as the spill displays high reflectivity of UV radiation even at thin layers. The UV instrument is not usable at night, and wind slicks, sun glints and biogenic material can cause false alarms in the UV data (Brekke and Solberg, 2005). These interferences are often different from those for TIR (Thermal Infrared), and a combination of TIR and UV can provide a more reliable indication of oil and can be used for estimating oil thickness (Fingas and Brown, 1997).

1.3.2. Visible

In the visible region of the electromagnetic spectrum oil has a higher surface reflectance than water and absorbs energy showing black or brown signatures but also shows limited nonspecific absorption tendencies (Nirchio et al., 2005). Oil generally manifests throughout this visible spectrum (Fingas and Brown, 1997). The use of visible techniques in oil slick remote sensing is restricted. Furthermore, the usefulness of systems working for oil detection on this spectrum is limited because they often cause mistakes due to sun glint, wind sheens and biogenic material (Fingas and Brown, 1997; Nirchio et al., 2005). Under highly favorable lighting and sea conditions man made oil slicks which are originated from ship accidents or platforms can be detected in the visible images (Brekke and Solberg, 2005).

1.3.3. Thermal Infrared

Oil absorbs solar radiation and re-emits a portion of this energy as thermal energy mostly in the range between 8–14 μm and emmisivity difference between oil (0.972 μm) and water (0.993 μm) leads to different brightness temperatures (Sabins, 1997). Therefore, oil layers appear colder than water in thermal images. Infrared sensors are also useful in evaluating the thickness of oil slicks. As the thickness increases they appear hotter in the infrared images and they can be distinguished from thin ones, however very thin layers can not be identified in thermal images (Fingas and Brown, 1997; Nirchio et al., 2005). At night a thick slick can appear cooler than the water since it releases heat quicker than its surrounding water. Thick and thin oil layers and the boundary between water and oil were possible to detect by the IR channel, but the oil slicks may not have a significant different temperature signature from the surrounding water at night (Brekke and Solberg, 2005).

1.3.4. Laser Flourosensors

Laser fluorosensors are active sensors that take advantage of the fact that certain compounds in petroleum oils absorb ultraviolet light and become electronically excited. This excitation is rapidly removed through the process of fluorescence emission, primarily in the visible region of the spectrum. Since very few other compounds show this tendency, fluorescence is a strong indication of the presence of oil (Fingas and Brown, 1997). The Airborne Laser Fluorosensor (ALF) was developed by British Petroleum's (BP) Research Centre during the 1980s as a means of identifying hydrocarbon seepage in frontier basins around the world (O'Brein et al., 2005). ALF is an extremely sensitive tool and detects the presence of thin (<1 micron) hydrocarbon films on the sea surface. Fluorescence lidar sensors are complementary, regarding the different thickness ranges that can be estimated by both sensors (Lennon et al., 2005).

1.3.5. Hyperspectral Sensors

Hyperspectral sensors used for oil spill monitoring have a potential for detailed identification of materials and better estimation of their abundance. With more than 200 wavelengths provided by a hyper spectral sensor, the spectral signature of oil can be exploited and used to distinguish between different oil types (Brekke and Solberg, 2005). Hyperion is an example of a space borne technology for hyper spectral remote sensing that was launched in 2000. Hyperspectral data would allow a better spatial resolution to be reached, but could not be used during night flights (Lennon et al., 2005)

1.3.6. Microwave Sensors

Microwave sensors are the most applicable tools for oil slick monitoring since they are not affected by clouds, haze, weather conditions and day/night differences. Different than shorter wavelengths of remote sensing systems, microwaves penetrate through atmosphere with very little absorption however; there are some exceptional cases for clouds and rain below 2 cm and 4 cm wavelengths respectively (Woodhouse, 2006). The most common microwave sensor for oil slick detection is the Synthetic aperture Radar (SAR). SAR image is a measure of surface roughness depending on the backscatter. The main mechanism in detection of oil slicks is the dampening effect of oil on water. Dampening of sea waves results in reduced radar return from the affected area, so that oil slicks appear as relatively dark features on the SAR scenes.

1.4. Purpose & Scope

So far; the sources, mechanisms and factors affecting the origin, migration, formation and spatial distribution of hydrocarbon seepages through the water column and sea surface as possible sources of naturally occurring oil slicks have been explained. Brief background information about the petroleum geology of the black sea has been presented. Available remote sensing techniques to detect these features giving more emphasis on SAR have been introduced. When the specific characteristics of the Black Sea in terms of meteorological conditions are considered, it is not as easy as

detecting oil slicks in calm waters. In other words the number of look-alikes (dark spots resembling oil slicks) will be much more and sometimes will lead false alarms. Consequently, selection of image accusation date and remote sensing techniques should be carefully made. When all these information are been taken into consideration, a research problem and research questions are defined.

The research questions for this study are;

1. How can we detect oil slicks with remote sensing?
2. What kind of methods can be used to classify them?
3. How can we evaluate the accuracy of the classification?

The main objective of this thesis is to develop a methodology for detection of naturally occurring offshore oil slicks originating from hydrocarbon seeps using satellite Advanced Synthetic Aperture Radar (ASAR) imagery. Offshore Central Black Sea is selected as a test area to implement the developed methodology. In order to achieve the presented research objectives the following working strategy will be followed:

- Adaptation of the present methodologies of SAR remote sensing to obtain more reliable results based on particular specific aspects of the Black Sea.

- Discrimination of the natural oil slicks from other phenomena called look-alikes creating dark spots on sea surface.

CHAPTER 2

SAR APPLICATIONS FOR OIL SLICKS

This chapter introduces principles and applications of synthetic aperture radar (SAR) for the purpose of offshore oil slick detection. The feature that makes SAR special for ocean remote sensing, where atmospheric conditions play important role, is the all weather capability. Satellite-based Synthetic Aperture Radar data is a low cost, regional tool that can provide an instantaneous radar snapshot of an area (O'Brien et al., 2005). Since SAR is the most common and appreciate method to detect offshore oil slicks many techniques have been developed. Parameters used to detect oil slicks are functions of radar configuration, slick nature and meteorological and oceanic conditions like height of the waves, the amount of oil that has been released, and the speed of the wind (Girard-Ardhuin et al., 2003; Espedal and Wahl, 1999). SAR has a great potential as well as some limitations. While applying classification procedures on radar imagery, the principles of imaging radar should be totally understood.

2.1. Principles of RADAR

RADAR is an acronym for Radio Detection and Ranging. Radar operates in the microwave portion of the electromagnetic spectrum. Imaging radars operates at a specific wavelength and frequency (Ryerson, 1998). Radar measures the time difference between the transmitted and received pulse. Radar image is a representation of the backscatter electromagnetic pulse, which is also called "echo", from the surface and the intensity of the pixel, and it is proportional to the surface roughness at the scale of Bragg Scattering (Ryerson, 1998; Allan 1983). The radar transmission equation for monostatic radar is defined as:

$$P_r = \frac{(\lambda G_d)^2 \sigma P_{rad}}{(4\pi)^3 r^4} \quad (4.1)$$

Where the variables are defined as shown in Table 2.1:

Table 2.1: Radar equation variables

Variable	Definition	Units
P_r	Time average power received by the radar antenna	watts (W)
λ	Wavelength of signal received by radar antenna	meters (m)
G_d	Directive gain of antenna (measure of the concentration of the radiated power in a particular direction)	unitless
σ	Radar cross section (characterizes the target's ability to scatter or reflect energy)	square meters (m^2)
P_{rad}	Power dissipated through the characteristic impedance, Rrad, of the radar antenna	watts (W)
r	Distance measured from the radar to the target	meters (m)

The periodic surface scatters in a number of directions given by the demand on constructive interference for reflections from two points separated by the periodicity "λ" illustrated in Figure 2.1 (Woodhouse, 2006). This relation is related to Bragg-scattering in crystals, and the relation is called the Bragg-resonance (Allan, 1983). Constructive interference is obtained in those directions where the difference in path length is a multiple of a wavelength. For the special case of back-scattering basic formula is obtained:

$$\Lambda = n \cdot \lambda / 2Sin\Phi_i \quad (4.2)$$

Where;

- Λ = periodicity
- Φi = incidence angle
- λ =wavelength

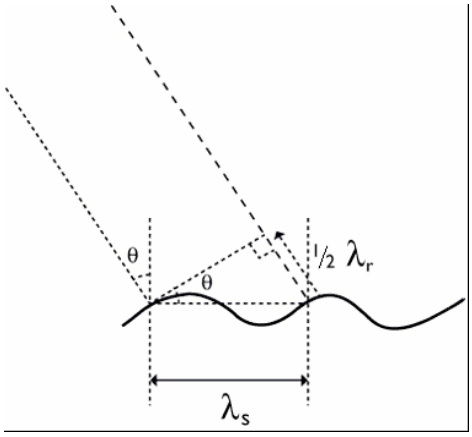

Figure 2.1: Illustration of Brag Scattering with periodicity

For the advanced synthetic aperture radar onboard the ENVISAT satellite (Φi = 19.2°-26.2°, λ=5, 62 cm) thus, a periodicity of Λ= 6.36 to 8.54 cm is obtained, which is the wavelength of short capillary/gravity waves, which are then mainly responsible for the scattering from oceans. These waves are strongly influenced by the wind and the backscatter to the satellite is then related to the wind speed and direction. However if there is an oil spill on the sea the capillary waves are damped out and there is very little backscatter (Solberg et al., 2007).

One other important principle of SAR is the “Polarization”. It is the orientation of the electromagnetic field and is a factor in the way in which the radar signal interacts with ground objects and the resulting energy reflected back. Electromagnetic radiation consists of an electrical field (E) which varies in magnitude in a direction perpendicular to the direction in which the radiation is traveling, and a magnetic field (M) oriented at right angles to the electrical field. Both these fields travel at the speed of light (c).Most radar imaging sensors are designed to transmit microwave radiation either horizontally polarized (H) or vertically polarized (V)**,** and receive either the horizontally or vertically polarized backscattered energy (Figure 2.2).

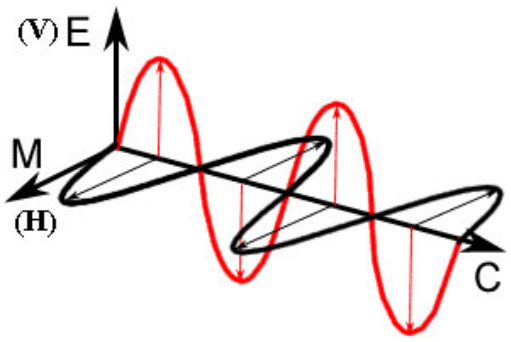

Figure 2.2: Behavior of Electromagnetic radiation (Source: CCRS/CCT)

2.2. Fundamentals of Oil Slick Detection with SAR

SAR is an active sensor which emits its own electromagnetic pulse and receives the backscattered signal. Radar backscatter coefficient is a function of the viewing geometry of the SAR and decreases with the increase of the incidence angle, and the scattering properties of a material depend on the polarization of the incoming radar signal (Allan, 1983). The main mechanism in detection of oil slicks is the dampening effect of oil on water which is explained by a lower backscatter from the sea surface because of “Bragg Scattering”.

Since the image brightness is a reflection of the microwave backscattering properties of the surface, it can be used to map natural and anthropogenic oil slicks, and to a lesser extent condensate slicks via the dampening effect of the liquid hydrocarbons on wind-induced rippling. This dampening results in reduced radar return from the affected area, so that oil slicks appear as relatively dark features on the SAR scenes. Gas can only be mapped rarely using SAR data, typically when it is associated with condensate (O’Brien et al., 2005). Radar backscattering level is decreased with slick, which appears as a dark patch with weak backscattering in comparison with surroundings in radar image (Girard-Ardhuin et al. 2003).

Even though a variety of methods are applied, the most appropriate method for detection of oil slicks is a combination of visual interpretation, automatic image processing and fuzzy expert classifier. Discriminative features of oil slicks and look-alikes are basically geometrical, radiometric

and textural. In addition to this, for the natural oil slicks there is one other discriminative feature which is temporal continuity. In other words, for the slicks to be naturally originated from subsurface the source of the seep should be permanent. Consequently, every slick should be present in a close neighborhood of the previously detected and classified slicks. However, orientation, shape and texture can be different because of the weather conditions at the time of image accusation.

The biggest difficulty, that makes oil slick detection from SAR images challenging, is the discrimination of look-alikes from oil slicks. Look-alikes are the natural and atmospheric phenomena that produce dark patches in SAR images similar to oil slicks. Look-alikes include natural organic films, grease ice, swirls, rain cells, and low wind speed areas of less than 3 m/s (Hovland et al., 1994; Solberg et al., 1999). Men made spills are also considered to be an oil slick and discrimination of these features are more difficult than look-alikes with textural and geometric features.

2.3. Satellite Configuration

Satellite configuration is the starting point for the oil slick detection procedure. There are 8 different satellites available for radar remote sensing and their configurations for polarization, spectral resolution and spatial resolution can be found in Table 2.2. Each frequency band is differently affected, function of wind speed and slick nature. Several experimental studies with multi-frequencies consisting of tipping artificial slicks have shown most important contrast with C, X and Ku-bands with *5* dB contrast for a slick made with “light” fuel, and 10 to 15 dB contrasts for a “heavy” fuel. Moreover, L and S-bands are weakly affected by slicks. Strong winds are a real problem to the damping measurement (Girard-Ardhuin et al., 2003).

In this study ENVISAT-ASAR images has been used. The Advanced Synthetic Aperture Radar (ASAR) instrument on board the ENVISAT satellite extends the mission of the Active Microwave Instrument (AMI) Synthetic Aperture Radar (SAR) instruments flown on the European Remote Sensing (ERS) Satellites ERS-1 and ERS-2. ASAR uses an active phased-array antenna, with incidence angles between 15 and 45 degrees. The sensor is emitting and receiving pulses from C-band (5 cm) of microwave wavelength.

Table 2.2: Satellite configurations for radar remote sensing.

Satellite	Operator	Launch Date	Resolution				Swath (km)
			Spectral (μm) S=Stereo	Spatial (m)	Radiometric	Temporal (days)	
SEASAT	NASA	1978	L-Band HH-polarization				
ALMAZ	Russia	1991	S- Band HH-Polarization				
JERS-1	Japan-NASDA	1992	L-HH (1.275 GHz)	18	3 bit	44	75
ERS-1	ESA	1992	C-VV (5.3 GHz)	30		35	100
ERS-2	ESA	1994	C-VV (5.3 GHz)	30		35	100
Radarsat-1	CSA	1995	C-HH band 16 beam mode (S)	100		24	50-500
ENVISAT	ESA	2002	C-VV, C-HH (5.3 GHz)	30		35	56-105
Radarsat-2	CSA-MDA	2003	C-HH, W,HV,VH	100		24	20-500

The spatial resolution of the sensor is 30 m. There are seven different possible swath widths for the image accusation ranging from 56 km to 105 km. ENVISAT-ASAR also provides polarization alternatives of vertical-vertical (VV), horizontal-horizontal (HH) and cross polarization alternatives like horizontal-vertical (HV) and vertical-horizontal (VH). These combinations represent the emitted and received electromagnetic pulse directions. In the stage of image ordering from ENVISAT first thing to do is the selection of operation mode. The operation modes are image mode (IM), and alternating polarization (AP). Secondly, polarization alternatives which have been mentioned above image level (Level 0 or Level 1) should be selected. Finally swath width should be determined. Schematic representation of image ordering process can be found in Figure 2.3. For oil slick detection VV polarized, C-band, and notably with strong wind at incidence angles in the range of 20^{o} to 45^{o} gives better results (Brekke and Solberg, 2005; Mouche et al., 2005; Girard-Ardhuin et al., 2003; Girard-Ardhuin et al., 2005). In this study, Image Mode (IM), VV polarization, Level 1 Precision Image (PRI) and swath 2 found to be most suitable configuration.

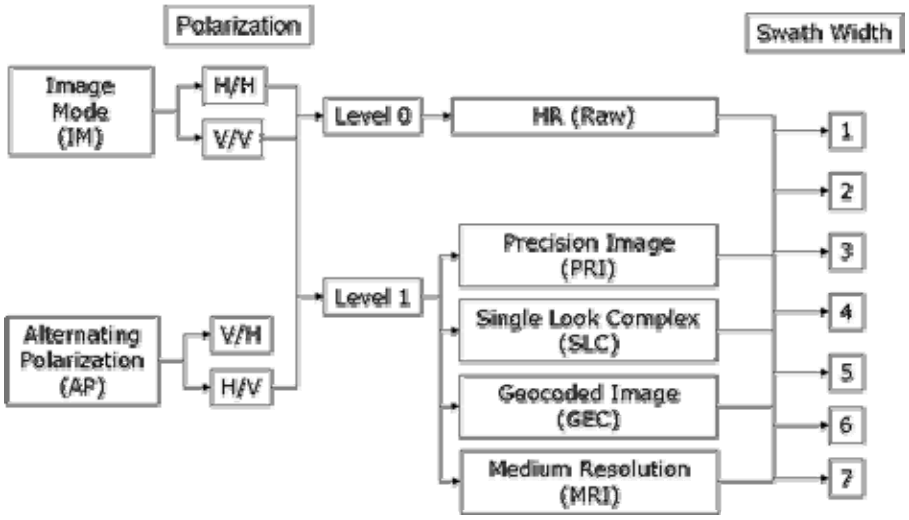

Figure 2.3: Scheme of ENVISAT-ASAR image ordering procedure.

2.4. Image Processing

There are different studies for oil slick detection from SAR images. One of the well-known studies made and later modified by Solberg et al. (1999), which consist of dark spot detection, feature extraction and slick classification stages. The basic approach in dark spot detection was filtering the image. Some of the filtering techniques that have been used in literature were cross-spectral phase filtering (Smith and Melger 2003), bayesian approach speckle filtering (Arvelyna et. al 2001), and Lee filtering (Karathanassi et al., 2006). In addition to these, statistical approaches have been applied to classify slicks and differentiate look-alikes. For instance fractionally integrated autoregressive-moving average has been used to discriminate of oil slicks from low wind areas (Bertacca et al, 2005), A probabilistic approach to distinguish oil spills from other similar oceanic features has been developed (Fiscella et al. 2000)

One of the most extreme methods was to compare different polarization measures applied to the detection of slicks to define their boundaries. Annealed segmentation of these measures is then employed to detect and define their boundaries including the intensity in a single polarization and the maximum eigenvalue and span measures for more than

one polarization channel (Lombardo and Oliver, 2000). Segmentation was also one of the most frequently used methods. Segmentation of oil slicks using a partial differential equation (PDE)-based level set method, which represents the slick surface as an implicit propagation interface was one of the approaches (Huang et al, 2005). Another one was auto segmentation with co-occurrence techniques (Arvelyna et. al 2001). Object based fuzzy classification has been used a continuation of segmentation and an alternative to probabilistic approaches for slick classification (Keramitsoglou et al. 2006). The summary of some of the representative studies for oil slick detection and classification including parameters used in image filtering, feature extraction and dark spot classification processes are represented in Table 2.3.

Table 2.3: Summary of oil slick detection techniques from various studies (Del Frate et al., 2000, Fiscella et al., 2000, Marghany 2004, Espedal and Wahl, 1999, Solberg et al., 2007).

FEATURES	Del Frate et al, 2000	Fiscella et al, 2000	Marghany 2004	Espedal and Wahl 1999	Solberg et al., 2007
Area	X	X		X	X
Perimeter	X	X		X	
Perimeter to Area Ratio		X			
Normalized Perimeter to Area Ratio		X			
Slick Width					X
Complexity	X	Form Factor			F. I. P. M.*
Spreading	X				
Object Standard Deviation	X				
Background Standard Deviation	X				
Contrast	X		X	X	X
Gradient	X			X	X
Gradient Standard Deviation	X				
Slick Radar Backscattering		X		X	
Outside Slick Radar Backscattering		X			
Intensity Ratio		X			
Standard Deviation Ratio		X			
Intensity Standard Deviation Ratio Inside		X			
Intensity Standard Deviation Ratio Outside		X			
ISRI to ISRO Ratio		X			
Shape Texture Based on Sub-objects				Texture	
Distance to a Point Source					X
Number of Detected Spot in the Scene					X
Number of Neighboring Spots					X
Homogeneity			X		X
Entropy			X		
Energy			X		
Correlation			X		

* First Invariant Planar Moment

CHAPTER 3

METHODOLOGY

This chapter introduces the materials and methods used for offshore oil slick detection with Synthetic Aperture Radar (SAR). Oil slick detection from SAR images usually framed into three fundamental levels; dark patch detection, features extraction, and oil slick classification (Solberg et al., 2007; Keramitsoglu et al. 2006; Nirchio et al. 2005). The methodology in this study is an adapted version of pre-existing techniques, consisting of three levels; two for dark spot detection and one for dark spot classification (Figure 3.1). First level is the visual interpretation level which includes removal of erroneous contrast trends, visual inspection of images and subset creation based on the locations of potential oil slicks. The second level includes the image processing and filtering operations. Third level which is the classification stage using object based classification techniques and fuzzy membership function to extracted features from image objects of segmented images. TNTmips software has been used for trend removal, subset creation, morphological filtering operations, and eCognitition software has been used for segmentation, feature extraction and object based classification processes.

3.1. Input Data Set Description

During the image processing and classification procedures of the study 10 different images of “ENVISAT ASAR Precision Image Mode Level 1” with Vertical-Vertical (V-V) polarization, Swath-2 (105 km) have been used from various dates. Although, the spatial resolution of the image is considered to be 30 meters, while converting radar signal to level zero precision image mode it is converted to a picture element of 12.5 x 12.5 meters. From the beginning of the study this rectangular picture element has been taken into account.

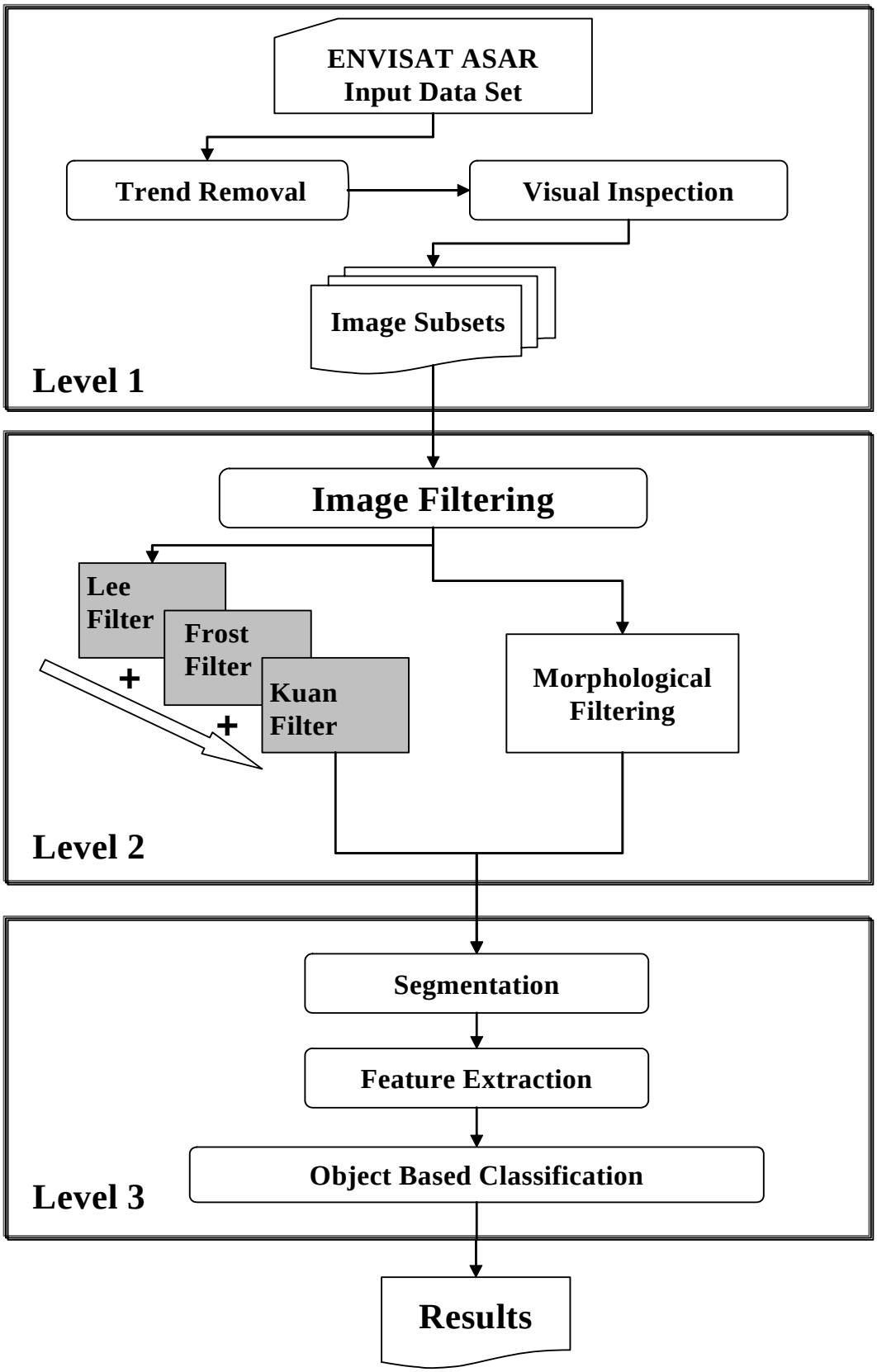

Figure 3.1: Flow Chart of the Methodology

Study area is very large and can be covered with 4 sets of ENVISAT-ASAR images. When the overlapping regions are taken into consideration the total area can be calculated as a rectangular area of 220 km x 160 km. Image selection has been done carefully in order to minimize the affect of surface roughness due to weather conditions. The details of data sets containing the information about date, time, orbit, track, frame and location of center each image can be found in Table 3.1.

Table 3.1: ENVISAT-ASAR Input Dataset Information

ENVISAT-ASAR Input Data Set				
Date	**Time**	**Orbit**	**Track**	**Frame**
07 August 2004	07:55:33	12743	164	2745
23 August 2004	07:52:39	12972	393	2745
23 August 2004	07:52:24	12972	393	2727
23 July 2005	07:55:35	17753	164	2745
08 August 2005	07:52:39	17982	393	2745
08 August 2005	07:52:24	17982	393	2727
14 May 2005	07:55:34	16751	164	2745
14 May 2005	07:55:20	16751	164	2727
25 April 2005	07:52:25	16479	393	2745
25 April 2005	07:52:42	16479	393	2727

3.2. Level-1 Visual Inspection

To start with, trend has been removed from ENVISAT-ASAR level zero images. In general, raster objects contain erroneous contrast trends introduced by the collection device or by the geometric orientation of the instrument (TNTmips, 2001). Trend Removal process is a polynomial surface fitting technique to remove systematic variations from monochrome raster objects (TNTmips, 2001). After trend removal the image is cleared from trend and became ready for further visual inspection and processing. De-trended images have been scanned visually to determine the target areas.

A trained human interpreter is able to discriminate between oil slicks and look-alikes based on experience and prior information concerning location, external information about weather conditions, differences in shape and contrast to surroundings between oil slicks and look-alikes (Solberg et al., 1999; Fiscella et al., 2000). The human eye is superior in observing a slick in the context of the surrounding sea. If the surroundings are homogeneous, the human observer will have more belief in that the spot is an oil slick than with heterogeneous surroundings (Solberg et al., 1999). With heterogeneous surroundings, the human eye can easily determine if the spot is separated from the surroundings based on contrast or orientation. External information about wind speed and direction, location of oilrigs and pipelines, national territory borders and coastlines can be used to support the analysis. Subset images have been extracted based on target areas containing dark spots on the bases of contrast level to the surroundings, homogeneity of the surroundings, wind patterns, nearby bright spots of ships, edge and shape characteristics for natural slicks.

3.3. Level-2 Image Filtering

Image filtering level aims at reducing speckle and enhancing the image. There are several ways to reduce speckle like increasing bandwidth of the radar system or reconstructing pixels through the averaging of the range line returns in the along track direction. However, these methods are applied during the image production and can not be controlled by the analysts. There are several filters and algorithms for reducing the speckle and convert the image into more interpretable form. Lee, Kuan and Frost Filters are three of them which have been used in the adaptive filtering stage of the SAR images.

The subsetting in the Level-1 has been followed by image filtering level which includes two steps; one step is the successive filtering of image with Lee, Frost and Kuan Filters for the removal of noise and speckle from the subset images, where the other step is a morphological filtering to emphasize morphology of the dark spots in the image. In terms of minimum loss of textural information and preserving edges, frost filter with 3 by 3 kernels is considered to give better results (Almeida-Filho et al., 2004). The

kernel is a window or matrix that applies the algorithm to pixels within defined frame.

The first approach was successive filtering of the image with Lee, Frost and Kuan algorithms, which has given a clear output for discrimination of dark areas from the remaining heterogeneous surroundings. The sequence of applied algorithms is not so important because all of these three filters aim to remove noise without disturbing the edges and sharp features. The reason why three of them are used successively is to remove the speckles that omitted by one of the filters. Lee algorithm smoothes speckled data based on minimum mean square error principle, Frost algorithm uses exponentially dampened convolution kernel and local statistics and Kuan algorithm applies minimum square error criterion after transforming multiplicative noise model into signal dependent additive noise model.

3.3.1. Lee Algorithm

Lee filter smoothes noisy or speckled data based on minimum mean square error principle by approximating the multiplicative noise model to a linear model. It has variations of additive and multiplicative components. The Algorithm is implemented by sliding a rectangular window with an odd length by selected window size in the two dimensions over the image (Marghany 2001). Lee filtering is a standard deviation based (sigma) filter that filters data based on statistics calculated within individual filter windows. Unlike a typical low-pass smoothing filter, the Lee filter and other similar sigma filters preserve image sharpness and detail while suppressing noise (Lee 1980). The pixel being filtered is replaced by a value calculated using the surrounding pixels. The filtered image can be given by;

$$\bar{i}(x,y) = I(x,y)w(x,y) + \bar{I}(x,y)(1 - w(x,y)) \tag{3.1}$$

$$w(x,y) = \frac{1 - C_{si}^2}{C_i^2(x,y)} \tag{3.2}$$

$$C(x,y) = 1 - \frac{\sigma(x,y)}{\bar{I}(x,y)} \tag{3.3}$$

- C_{si} = the speckle index,
- C_i = the ratio of square root of local variance over the local mean
- I(x,y) = the pixels which will be filtered
- $\bar{I}$ (x,y) = the output pixel
- σ = the standard deviation of intensity within window
- w = the weight for each pixel

3.3.2. Kuan Algorithm

The Kuan filter is primarily used smoothing radar image data without removing edges or sharp features in the image. It is only applicable for radar intensity image. The algorithm applies minimum square error criterion after transforming multiplicative noise model into signal dependent additive noise model (Kuan et al. 1985). The results are very similar to Lee filtering with weighing function difference. Kuan Filter can be considered to be superior to Lee filter since it does not make any approximation to the original model (Kuan et al. 1985). The resulted gray level R for the smoothed pixel is;

$$R = I_c \times \omega + \mu \times (1 - \omega) \tag{3.4}$$

$$\omega = \frac{(1 - \frac{C_u^2}{C_i^2})}{(1 + C_u^2)} \tag{3.5}$$

$$C_u = \sqrt{1/\ N_{Look}} \tag{3.6}$$

$$C_i = \frac{\sigma}{\mu} \tag{3.7}$$

- C_i = the ratio of Standard deviation of intensity within window over the local mean.
- N_{Look} = Number of Looks
- I_c = Center Pixel in Filter window
- μ = mean value of the intensity within window
- σ = Standard deviation of intensity within window
- ω = Weight for each pixel
- C_u= the root square of the reciprocal of the Number Looks.

3.3.3. Frost Algorithm

Frost filter helps to reduce speckle while preserving edges in radar images using exponentially dampened convolution kernel and local statistics

(Frost et al.1982). The pixel being filtered is replaced with a value calculated based on the distance from the filter center, the damping factor, and the local variance. Frost filter is different from Lee and Kuan filters regarding the estimated scene reflectivity by convolving the observed image with impulse response of the SAR system. The resulting value R for the smoothed pixel is;

$$R = \frac{\sum_{i=1}^{n} P_i \times \omega_i}{\sum_{i=1}^{n} \omega_i} \tag{3.8}$$

Where;

$$\omega_i = EXP \quad (-A \times T_i) \tag{3.9}$$

$$A = D \times (\frac{\sigma}{\mu})^2 \tag{3.10}$$

- A = Exponential Damping Factor
- μ = mean value of the intensity within window
- σ = Standard deviation of intensity within window
- T_i= Absolute value of the pixel distance from the center pixel to its neighbors in the filter window.
- P_i= Grey level for each pixel in filter window.
- ω = Weight for each pixel

3.3.4. Morphological Filtering

Second approach was to apply morphology filters on the subset images. In order to apply a morphology filter the radiometric resolution of subset images should be reduced down to regular 8-bit, as the SAR images are coded in 32 bit floating point pixel values with most of the image values are concentrated in a compressed part near zero. Morphological filtering is utilized based on geometry and the shapes within images in its processes. Morphological transformation simplifies the image and enhances object structure, while maintaining the primary shape characteristics within the object. Most common morphological functions are Dilation, Erosion, Opening, Closing, Clump, and Sieve (TNTmips, 2001). These functions affect the shape of the file without disturbing the raster size.

Dilate function is a function of filling, expanding, or growing. It fills the holes smaller than the structural element or the kernel in a binary or gray scale image. This function can be used to join the separated dark spot after thresholding. In other words it may retain the original shape of the dark spot as much as possible (Gonzales and Richards 1992, Russ 1992). On the other hand erode function does the reverse of dilate function. It removes the unwanted islands of pixels within the kernel. This may also be useful in some situations. Opening function is defined as the erosion of the image followed by subsequent dilation using the same structural element which smoothes the contours, breaks narrow isthmuses, and eliminates small islands and sharp peaks or capes in an image (TNTmips, 2001). Similarly Closing function defined as the dilation of the image followed by subsequent erosion using the same structural element which smoothes the contours fuse narrow breaks and long thin gulfs, eliminates small holes, and fills gaps in the contours of an image (Gonzales and Richards 1992, Russ 1992). The selection of these functions should be decided by the analysts. The Clump and Sieve morphological functions work a bit differently than the other four functions. These two functions use groups of contiguous cells that have the same raster cell value rather than structural elements (Sonka et al. 1993). They may not be very useful for dark spot detection. Among four common morphology filters are erode, dilate, opening and closing filters. Throughout these filters, opening filter has been selected, because it applies an erode filter followed by a dilate filter aiming to join the inliers to the super-object in the frame of the filter kernel.

3.4. Level-3 Object Based Classification

Object oriented classification is different then traditional image classification techniques since it deals with objects rather than single pixels. Object based classification starts with segmentation and followed by feature extraction from segment and finalize with membership function definition based on extracted features and classification based on defined hierarchy.

3.4.1. Segmentation

The first process of this stage is segmentation which allows knowledge free extraction of homogeneous image object primitives in any chosen resolution, especially taking into consideration local contrasts (eCognition, 2004). It generally can be applied to a very large range of data types; it works on an arbitrary number of channels simultaneously and is especially suited for textured or low contrast data such as radar. There are several methods for image segmentation but they are mainly split into two domains: knowledge driven methods (top-down) and data driven methods (bottom-up). In top-down approaches, the system tries to find the best methods of image processing to extract segments (eCognition, 2004). In bottom-up approaches the segments are generated based upon a set of statistical methods and parameters for processing the whole image (eCognition, 2004).

Generally throughout different types of texture segmentation algorithms the modeling and the optimization stages has been followed (Mao and Jain 1992, Hofmann et al. 1998, Haralick et al. 1973). In the modeling stage characteristic features are extracted from the textured input image and range from spatial frequencies and co-occurrence matrices to wavelet coefficients, wave packets and fractal indices. In the optimization stage features are grouped into homogeneous segments by minimizing an appropriate quality measure. This is most often achieved by a few types of clustering cost functions.

Two input layers have been used for the segmentation. For the first layer the subset image has been filtered successively with Lee, Frost and Kuan algorithms. The second input layer is morphologically filtered 8 bit image. Different weight parameters have been assigned to input layers depending on their importance or suitability for the segmentation result. Higher weight has been given to the layer from which, more information will be used during the segmentation process. Segmentation may also be done from one layer but better results can be achieved results if more than one layer is used (eCognition, 2004).

The segmentation has been generated based upon several adjustable criteria, like shape factor, scale parameter, smoothness and compactness. The scale parameter determines size of the resulting image objects. In this

study larger scale parameter has been used for heterogeneous subset scenes and conversely smaller scale parameter has been used for homogeneous subset scenes. The shape factor helps to avoid a fractal shaping of objects in strongly textured radar data and improves quality of object extraction. The smoothness criterion optimizes image objects with regard to smooth borders. Smoothness is a very important parameter when working on very heterogeneous radar images in order to maintain non-compact objects. The compactness criterion is inversely related to smoothness and used to optimize image objects with regard to compactness to identify object with relatively weak contrast. A strong and experienced source for the evaluation of segmentation techniques is the human eye. The results of the segmentation are supervised until satisfactory segmentation is achieved.

3.4.2. Feature Extraction

After segments have been created, features related to “layer values”, “shape” and “texture” have been computed for each segment (Table 3.2). Important features related to layer values are; mean layer value, mean brightness value, Minimum and maximum pixel value, mean difference to neighbor pixels, and mean difference to scene. Features related to shape for are; area, length to width ratio, compactness, and shape index. Features related to texture are; homogeneity, contrast, and dissimilarity.

Layer Mean Value: Mean value of the spectral mean values of an image object.

$$\bar{C}_L = \frac{1}{n} \cdot \sum_{i=1}^{n} C_{Li} \tag{3.11}$$

Brightness: Sum of the mean values of the layers containing spectral information divided by their quantity computed for an image object.

$$b = \frac{1}{n_L} \cdot \sum_{i=1}^{n_i} \bar{c}_i \tag{3.12}$$

Minimum and Maximum Value: Value of the image object's pixel with the lowest and highest value.

Table 3. 2: Summary of most frequent object features (eCognition, 2004).

Object Features		
Layer Values	**Shape**	**Texture**
Mean	Area	Homogeneity
Brightness	Length	Contrast
Max. Diffrence	Width	Dissimilarity
Standart Deviation	Length / Width	Entrophy
Ratio	Border Length	Angular Second Moment
Min. Pixel Value	Shape Index	Mean
Max. Pixel Value	Density	Standart Deviaation
Mean Difference to neighbors	Main Direction	Correlation
Mean Difference to brighter neighbors	Asymetry	Contrast
Mean Difference to darker neighbors	Compactness	
Relative Border to neighbors	Eliptic Fit	
Mean Difference to super objects	Rectangular Fit	
Standart Deviation to super object		
Mean Difference to scene		
Standart Deviation to scene		

Mean Difference to Neighbors: For each neighboring object the layer mean difference is computed and weighted with regard to the length of the border between the objects (if they are direct neighbors, feature distance = 0) or the area covered by the neighbor objects (if neighborhood is defined within a certain perimeter (in pixels) around the image object in question, feature distance > 0).

The mean difference to direct neighbors is calculated as follows:

$$\Delta c_L = \frac{1}{l} \cdot \sum_{i=1}^{n} l_{Si} \cdot (\bar{c} - \bar{c}_{Li}) \qquad (3.13)$$

- l = Border Length of the mage object of concern.
- l_{Si} = Border length shared with direct neighbor "*i*".
- $\bar{c}_L$ = layer mean value of the image object of concern.
- $\bar{c}_{Li}$ = layer mean value of neighbor "*i*".
- n = Quantity of neighbors.

Area: In non-georeferenced data the area of a single pixel is 1. Consequently, the area of an image object is the number of pixels forming it. If the image data is georeferenced, the area of an image object is the true area covered by one pixel times the number of pixels forming the image objects.

Length / Width: There are two ways to compute the length/width ratio of an image object. The first one is used when ratio length/width is identical to the ratio of the eigenvalues of the covariance matrix with the larger eigenvalue being the numerator of the fraction and the second one can be approximated using the bounding box.

$$y = \frac{1}{w} = \frac{eig_1(S)}{eig_2(S)}, \quad eig_1(S) > eig_2(S) \tag{3.14}$$

$$y = \frac{1}{w} = \frac{a^2 + ((1-f)\cdot b)^2}{A} \tag{3.15}$$

Shape Index: Mathematically the shape index is the border length "*e*" of the image object divided by four times the square root of its area *A*. Use the shape index s to describe the smoothness of the image object borders. The more fractal an image object appears, the higher its shape index.

$$s = \frac{e}{4\cdot\sqrt{A}} \tag{3.16}$$

Compactness: The density *d* can be expressed by the area covered by the image object divided by its radius. The eCognition uses following implementation, where *n* is the number of pixels forming the image object

and the radius is approximated using the covariance matrix: Use the density to describe the compactness of an image object. The ideal compact form on a pixel raster is the square. The more the form of an image objects is like a square, the higher its density.

$$c = \frac{n \cdot m}{a} \tag{3.17}$$

Texture related features can be extracted based on the grey level co-occurrence matrix (GLCM), which is a tabulation of how often different combinations of pixel grey levels occur in an image (Haralick, 1979). A different co-occurrence matrix exists for each spatial relationship. To receive directional invariance all 4 directions (0°, 45°, 90°, 135°) are summed before texture calculation. An angle of 0° represents the vertical direction, an angle of 90° the horizontal direction.

Homogeneity: "Homogeneity" weights the values by the inverse of the "Contrast" weight with weights, decreasing exponentially according to their distance to the diagonal. If the image is locally homogenous, the value is high if GLCM concentrates along the diagonal.

$$\sum_{i,j=0}^{N-1} \frac{P_{i,j}}{1+(i-j)^2} \tag{3.18}$$

Contrast: "Contrast" is the opposite of "Homogeneity". It is a measure of the amount of local variation in the Image. It increases exponentially as (i-j) increases.

$$\sum_{i,j=0}^{N-1} P_{i,j}(i-j)^2 \tag{3.19}$$

Dissimilarity: Similar to "Contrast", but increases linearly. High if the local region has a high contrast.

$$\sum_{i,j=0}^{N-1} P_{i,j}\left|i-j\right|^2 \tag{3.20}$$

3.4.3. Membership Functions

The last stage is defining membership function based on extracted features. For the classification procedure an object based fuzzy logic has been utilized. In order to discriminate dark spot areas, a simple class hierarchy has been constructed consisting two classes which are “Clear Sea Water” and “Dark Spots”. “Dark Spots” class includes two subclasses namely “Probable Oil Slicks” and “Probable look-alikes” (Figure 3.2).

Object features have been used in defining the boundaries of membership functions. Each extracted feature has a set of fuzzy expressions for logical operation, allowing discrimination of dark spots and clear water bodies, and estimation of the dark spot to be a “Probable Oil Slick” or “Probable Look-alike”. Fuzzy rule can have a single condition or can consist of a combination of conditions that have to be fulfilled for a dark object to be assigned to a probability class (Karathanassi et al. 2006).

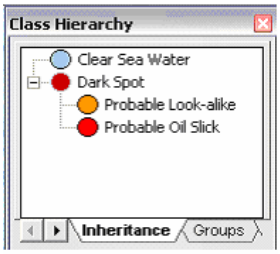

Figure 3.2: Class Hierarchy representing relation of classes and subclasses.

Fuzzification describes the transition from a crisp system to a fuzzy system. The membership value is defined by a so-called membership function. Membership function assigns a membership degree or value between 0 and 1 to each feature value. Boundaries of membership functions have been determined based on feature value intervals from randomly selected segment that are supposed to belong to a specific class. The shape of different kind of membership functions can be seen in Figure 3.3. In most of the cases “Boolean Range Function” has been used, which assigns a value of ‘1’ between specific values and assigns ‘0’ for the rest, in order to achieve sharp distinction of “Probable Oil Slick” and “Probable Look-alike” classes.

For successful classification a deliberate choice of membership function is crucial. This allows the introduction of expert knowledge into the system. The better the knowledge about the real system is modeled by the membership functions, the better the final classification result. In fuzzy classification methods, segments whose feature values are within these overlapping ranges can be seen as ambiguous objects and can belong to more than one classes but with different degrees of membership (eCognititon, 2004). Although it is possible to describe these ambiguities by making accuracy assesment calculation, the main aim is to define classes as unambiguously as possible.

As a final stage of all these classification stages an accuracy assessment has been done by Classification Stability and Best Classification Result. Classification Stability explores differences in degrees of membership between the best and the second best class assignments of each object, which can give evidence about the ambiguity of an object's classification. Best Classification Result is very similar to Classification Stability and determines whether object has memberships in more than one class. In the accuracy assessment of classification basic statistical information like number of image objects, mean, standard deviation, minimum value and maximum value have been calculated yielding an evaluation of fulfillment of class description. The accuracy assement can be done by calculating calss stability which finds the segments belonging to multiple classes and assigns an ambiguity level. Ambiguous objects are not misclassified objects, but there is no class to which these objects belong to explicitly. Thus, less ambiguous the objects gives more usable classification results.

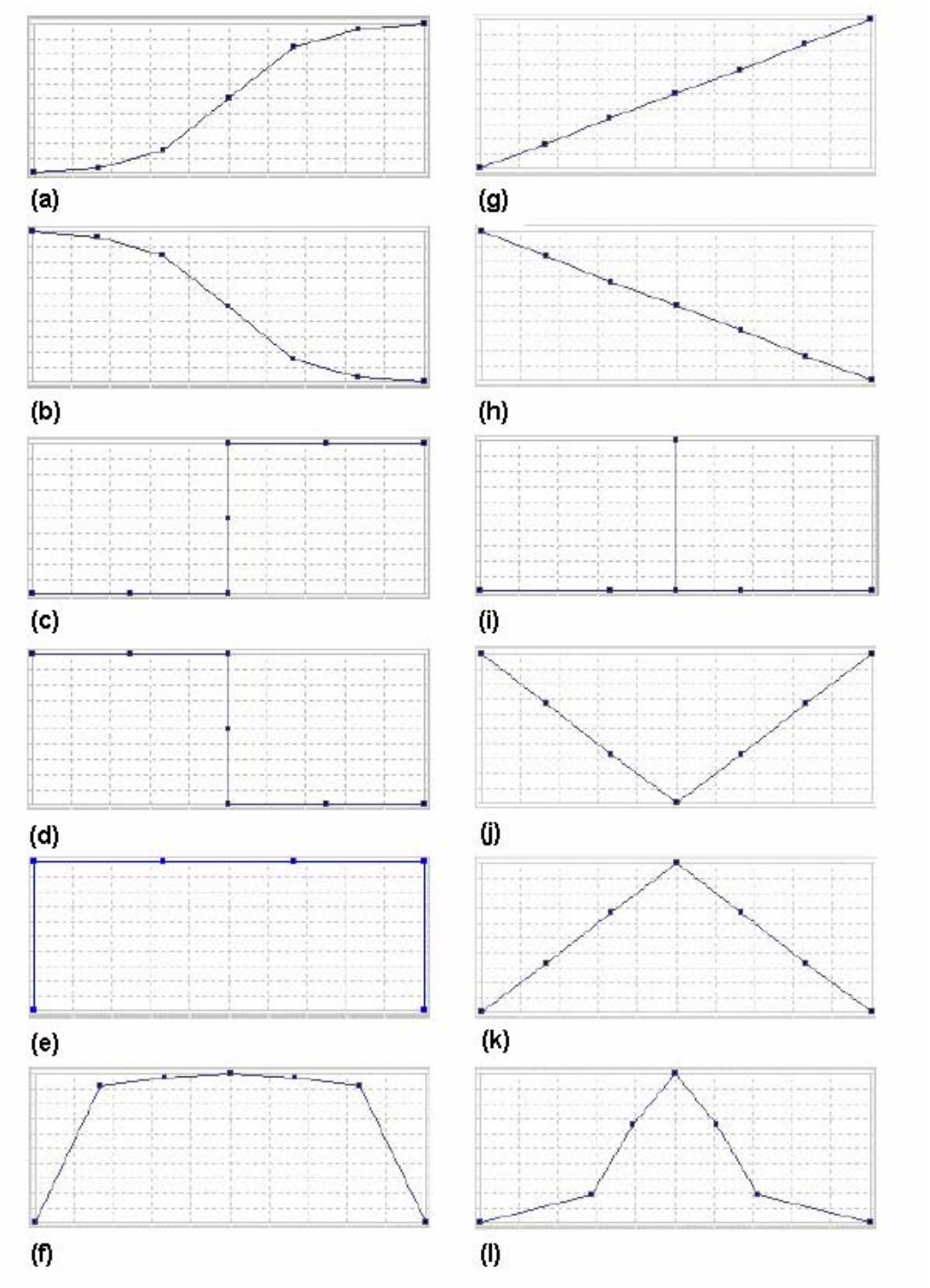

Figure 3.3: Typical Membership functions used in object based classification. a) Larger than, b) Smaller than, c) Larger than (Boolean), d) Smaller than (Boolean), e) Range (Boolean), f) About range, g) Linear Greater than, h) Linear smaller than, i) Singleton, j) Linear range (V), k) Linear range (upside V), l) Approximate Gaussian.

CHAPTER 4

RESULTS

4.1. Results of Visual Inspection

As it is explained in flow chart of the methodology in Chapter 5, the first level of the process is the visual interpretation of the images of which the trends had been removed. This level is named as Pre-Detection Stage since, except the trend removal process all the detection is based on human interpreter. Hence as the starting process, trend has been removed from the images in the order of 2 with a sampling rate including all lines and columns. After trend removal, 10 images from 6 different dates have been analyzed and are manually interpreted to detect the dark spot areas. As a result of visual interpretation, 61 dark spots have been detected as potential oil slick candidate. Based on these interpretations 16 subsets have been selected to be investigated in further stages (Figure 4.1).

At this level, all the detection parameters are pixel based and depend on the objectiveness of the interpreter. Before any object based classification the dark spots will not be called as oil slicks or look-alikes. It is also important to mention that the term “probable oil slick” will be used for all natural and man made oil related dampening affect of sea water. The first aim will be discrimination of “Probable Oil Slicks” from the “Probable Look-alikes”.

4.2. Results of Image Filtering and Classification

In this section of the chapter the results obtained from image subsets will be presented. The findings of the image filtering, segmentation, object based classification and accuracy assessment will be discussed. Throughout 16 subsets, 20 scenes with 1024 x 1024 pixel sizes have been selected and three different cases of dark spot occurrences have been identified.

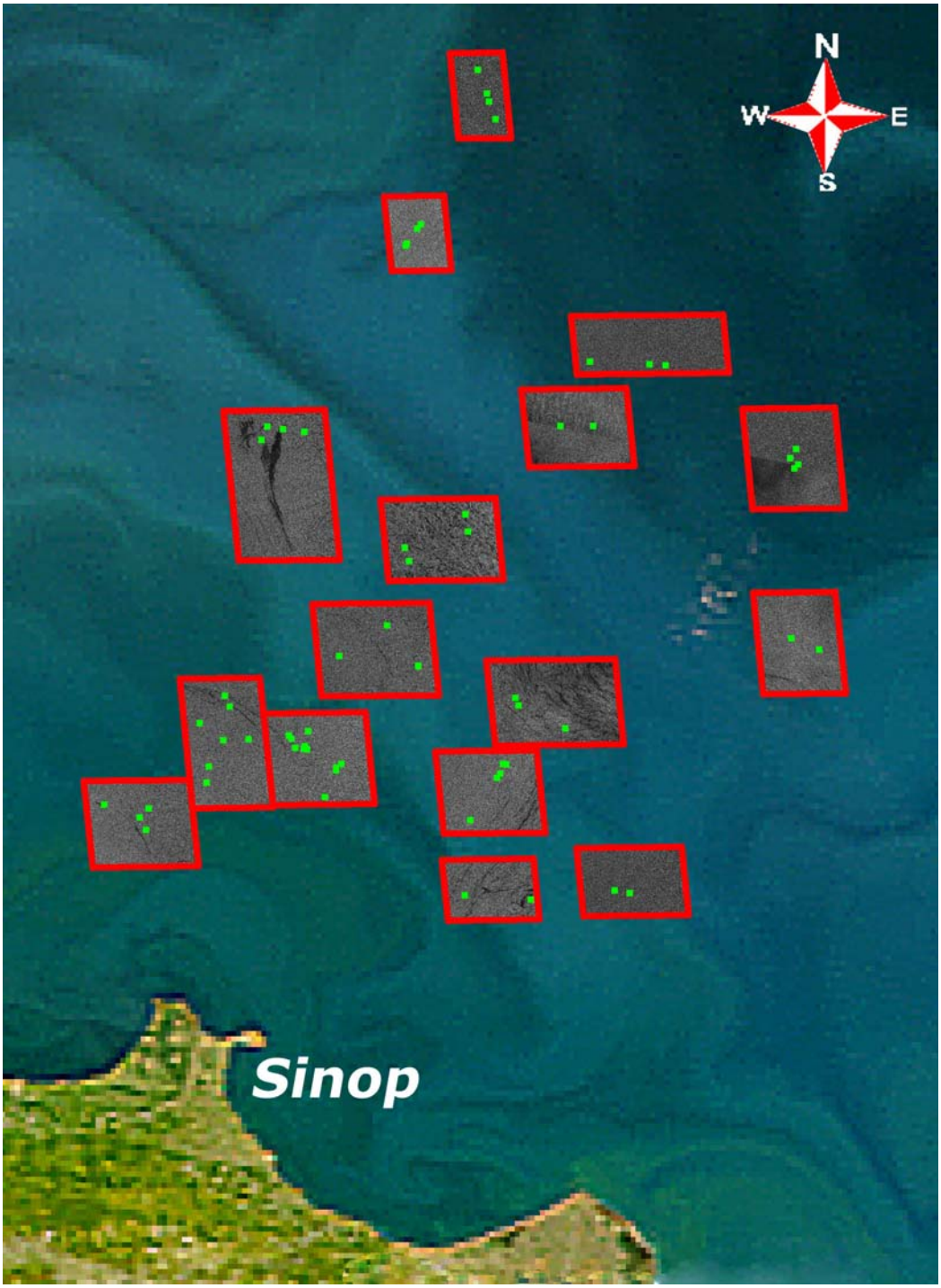

Figure 4.1: Results of Visual Inspection level, representing slick locations and extracted subset images.

First case is characterized by dark spots oriented in different direction and different contrast values. The second case includes darks spots oriented in a single direction but having darker surroundings than the first case. The third case is contains dark spots isolated from the surroundings in homogeneity, contrast and shape. As a result, 6 out of 20 scenes are categorized as “Case 1”, 11 out of 20 as “Case 2”, and 3 out of 20 as “Case 3” (Table 4.1).

Table 4.1: Category description for the three different cases of dark spot occurrences

Categories	Number of scenes	Category Description	
		Dark Spot Orientation	Contrast to Surroundings
Case-1	6	multi-directional	Moderate
Case-2	11	Uni-directional	low
Case-3	3	Uni-directional	High

4.2.1. Case 1

First case includes dark spots with different orientations and different contrast with the surroundings. The best example of this category has been selected for visual presentation. Firstly, the standard procedure, successive filtering by Lee, frost and Kuan algorithms, has been applied to subset scene (Figure 4.2). This successive filtering let the speckle to be removed from the image and more smoother output achieved. Secondly, radiometric resolution of the subset image is changed to 8-bit and then an opening morphological filter is applied (Figure 4.3).

For the segmentation of subset 1, a weight parameter of ‘2’ has been given to 8-bit morphology filter layer and ‘1’ has been given to speckle filter image. Segment scale parameter has been decided as 20 after several trials. Shape factor has been set to 0.4. Smoothness parameter has been set to 0.7 yielding compactness to be automatically 0.3 (Figure 4.4).

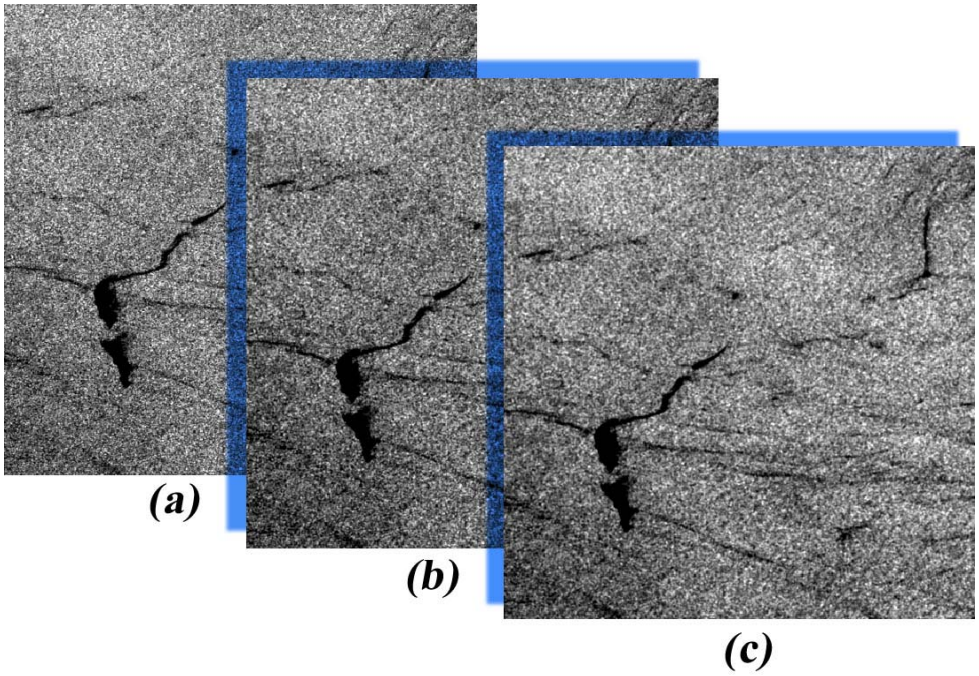

Figure 4.2: Successive Speckle Filtering of subset image sample scene for Case 1, (a) Lee algorithm, (b) Lee + Frost algorithm, (c) Lee + Frost + Kuan algorithm.

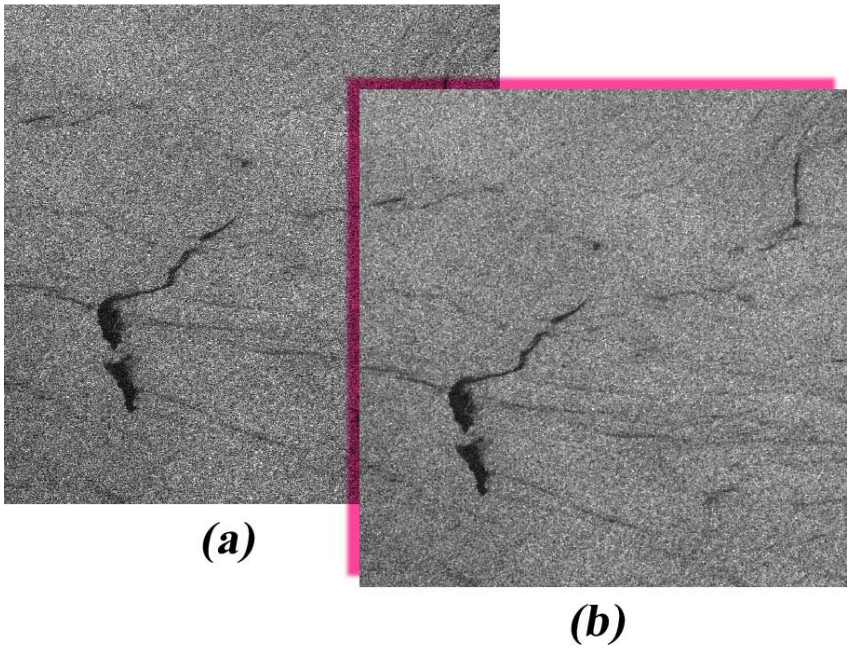

Figure 4.3: (a) Radiometrically rescaled 8-bit subset image 1, (b) Opening morphology filter applied subset image sample scene for Case 1.

After segmenting the subset image some specific features related to layer values", "shape" and "texture" has been automatically calculated for each segment (Figure 4.5). Sample segments have been selected randomly, which are supposed to belong to one specific class. The interval of feature values has been determined and tabulated in Table 4.2 by checking sample segments' feature values.

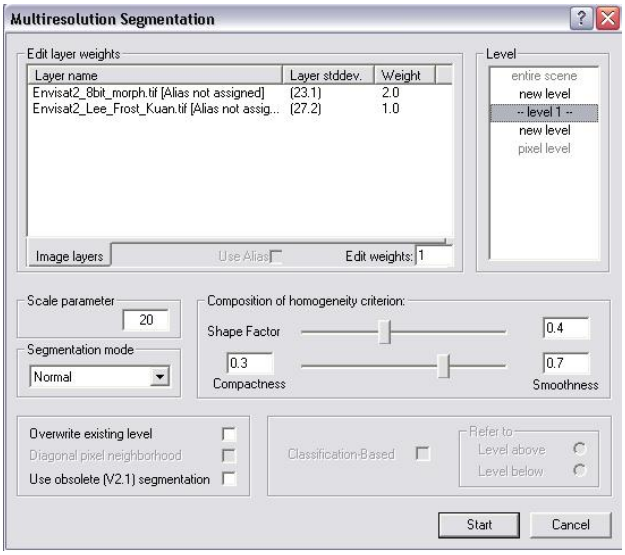

Figure 4.4: Parameters used for image segmentation of subset image sample scene for Case 1.

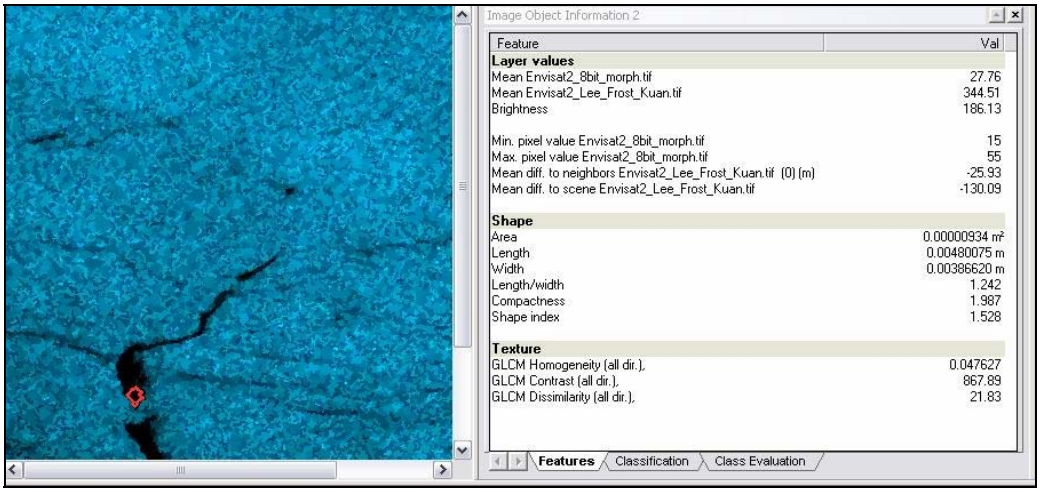

Figure 4.5: Features extracted from one segment indicated by the red highlight.

Table 4.2: Features extracted from randomly selected sample segment representing ranges for membership boundaries of subset image sample scene for Case 1.

FEATURES	Membership Boundaries		
	Oil Slick	Look-alike	Clear Sea Water
Mean Layer Value (8-bit Morph.)	25-40	55-75	80 - 125
Mean Layer Value (Lee-Frost-Kuan)	230-370	400-430	438 – 502
Brightness	180-210	230-260	257 – 315
Min. Pixel Value (8-bit-Morph)	10-25	35-50	44 – 89
Max. Pixel Value (8-bit-Morph)	50-60	90-155	146 – 89
Mean difference to Neighbor Pixels	(-32) - (-15)	(-42) - (-29)	(-12) – 30
Mean difference to Scene	(-132) - (-105)	(-62) - (-42)	(-34) – 25
Area (meter square)	130 - 1550	90 - 700	300 – 1500
Length / Width	1,5 – 6,6	1,9 – 4,7	1,2 – 1,7
Compactness	1,4 – 2,4	1,9 – 2,3	1,5 – 1,9
Shape Index	1,5 – 2,9	1,4 – 2,5	1,1 - 2,2
Homogeneity	0,038-0,048	0,037-0,042	0,038 – 0,053
Contrast	860-1280	1170-1405	1050 – 1350
Dissimilarity	20-27	25-29	24 – 27

Based on the extracted features tabulated in Table 4.2 membership functions has been defined for the class hierarchy represented in previous sections. For class “Dark Spot” a Boolean range membership function has been defined using minimum pixel value morphologically filtered image. Since “Probable oil Slick” and “Probable Look-alike” classes are subclasses of “Dark Spot” class this membership function appears to be an inherited function for them and the rules are valid for the subclasses as well. For the subclasses contained membership functions have been defined using information from brightness, homogeneity, dissimilarity, mean difference scene, mean difference to neighbor pixels, and standard nearest neighborhood function mean values of input layers. Logical operator “and” has been used to take the intersection and “or” has been used to take the union of membership function (Figure 4.6). The image is classified based on the membership functions but some segments are found to be unclassified. In order to correct unclassified areas the membership function and logical operators are modified and tweaked for intersecting boundaries of feature

values. Finally the resultant classified image is obtained and presented in Figure 4.7.

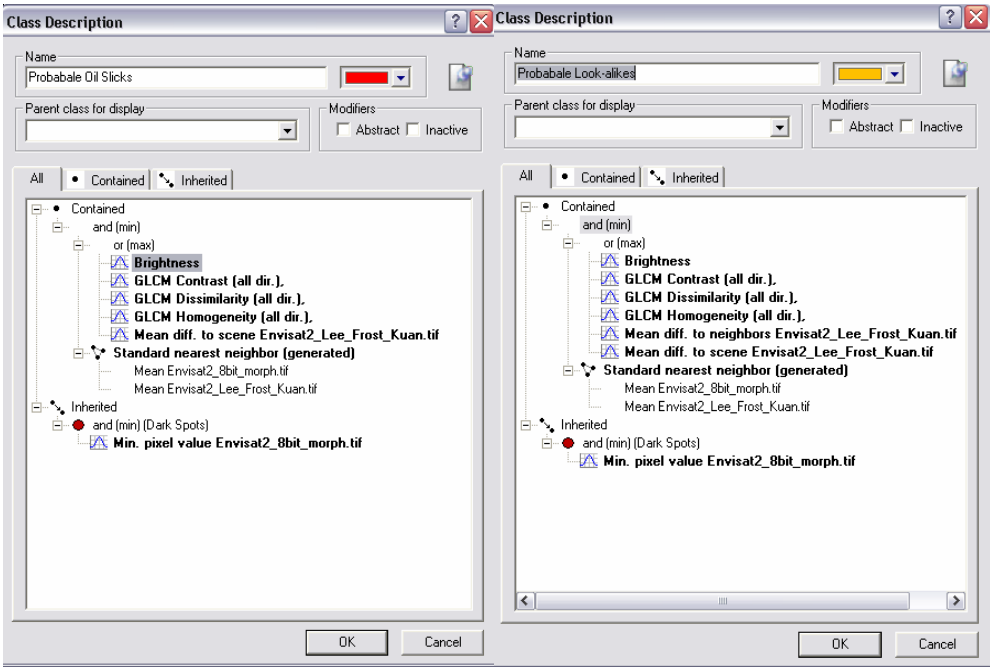

Figure 4.6: Class Description showing features used membership functions for subset image sample scene for Case 1.

Last stage after classification is the accuracy assessment. 'Classification Stability' and 'Best Classification Results' method has been used to evaluate the accuracy of the classes. As a result of 'Classification Stability' 39 segments out of 6347 have been classified as "Probable Oil Slicks" with an accuracy of 90 %, 213 segments have been classified as "Probable look-alikes" with an accuracy of 95 %, and 6095 segments have been classified as "Clear Sea Water" with an accuracy of 98 % (Table 4.3).

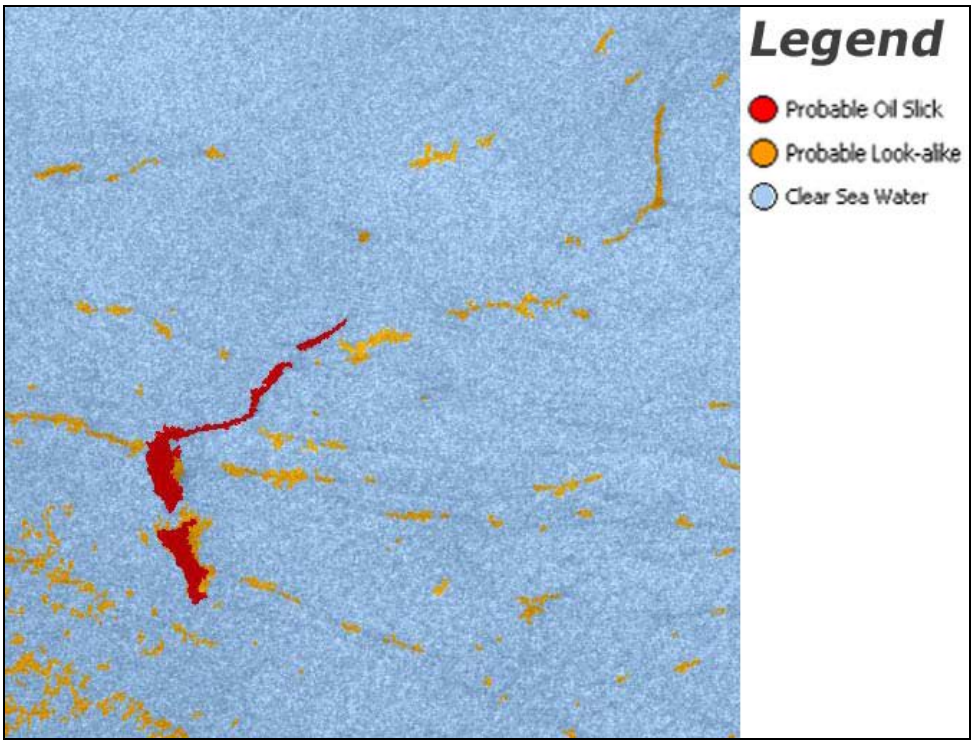

Figure 4.7: Classified subset image sample scene for Case 1 representing the discrimination of two dark spot classes.

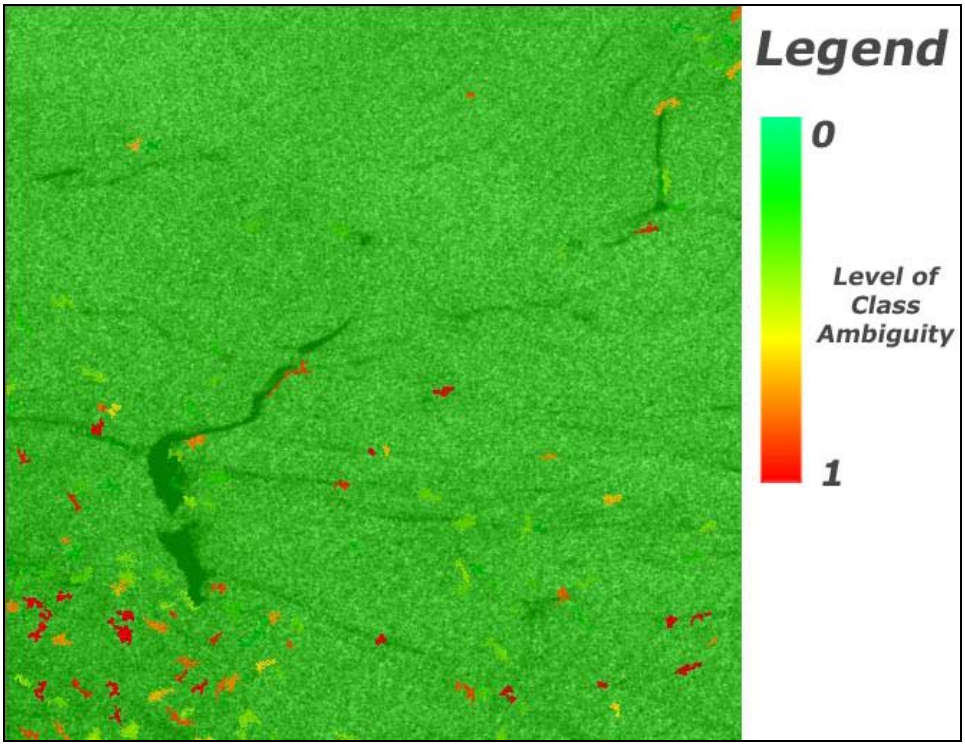

Figure 4.8: Visual Display of Class Stability Accuracy Assessment for subset image sample scene for Case 1.

Moreover, 'Best Classification Results' showed that 99 % of segments belonging to "Probable Oil Slicks" has only one class, similarly, probability of segments belonging to "Probable look-alikes" "Clear Sea Water" are 98 % and 100 % respectively. The visual display of accuracy assessment presented the level ambiguity of segments belonging to the assigned class can be seen in Figure 4.8. Green color represents zero percent ambiguity whereas red color shows a complete ambiguity in the classification.

Table 4.3: Results of Accuracy Assessment for subset image sample scene for Case 1

	Classification Stability				
CLASS	**Objects**	**Mean**	**Std. Dev.**	**Min.**	**Max.**
Probable Oil Slick	39	0,9070	0,199	0,1105	1
Probable Look-alike	213	0,9504	0,1319	0	1
Clear Sea Water	6095	0,9804	0,1246	0,0021	1

4.2.2. Case 2

The second case includes darks spots oriented in a single direction and the contrast differences between dark areas are les the first case. That makes the situation a little bit complex. As it is in the first case image filtered by Lee-Frost-Kuan algorithms and 8-bit morphological filtered image has been used as input and segmented image has been obtained with a scale parameter has been decided as 20, Smoothness parameter of 0.7, compactness parameter of 0.3 and shape factor of 0.4 (Figure 4.9).

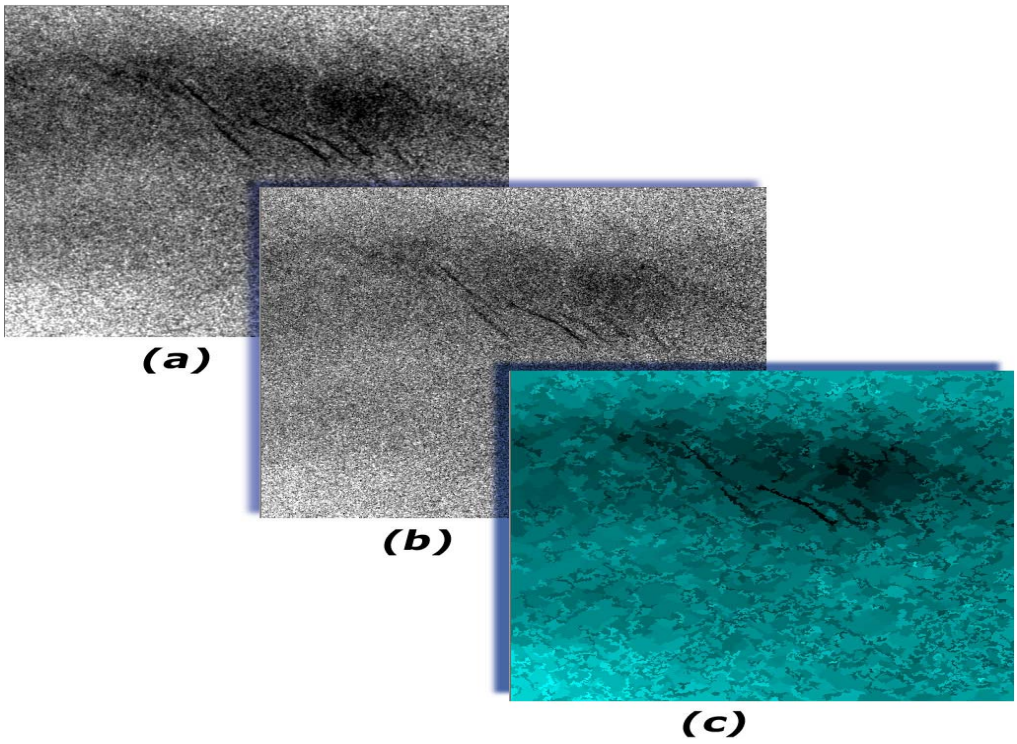

Figure 4.9: Input and output images of segmentation from sample scene for Case 2, (a) Lee + Frost + Kuan algorithm, (b) 8.bit morphology filter, (c) Segmented image

Similar to the previous case Boolean range membership functions has been defined for minimum pixel value of 8-bit input image, mean difference to scene, length to width ratio, compactness, shape index and brightness (Table 4.4). Different point in the second case is the impact of shape of the segments. In the first case the features related to shape have been computed but not taken into account since they have not been found to be representative. However, in this case texture feature are not representative since the values are very close and coinciding with each other (Table 4.4). Homogeneity, contrast and dissimilarity values are very close to each other. Similarly, 'mean difference to scene' values are not very useful to discriminate two types of dark spots. Consequently, the image is classified based on layer values and shape features (Figure 4.10). When accuracy assessment of the classification completed it has been found that 38 segments out of 6894 have been classified as "Probable Oil Slicks" with an accuracy of 65 %, 420 segments have been classified as "Probable look-alikes" with an accuracy of 79 %, and 6436 segments have been classified

as “Clear Sea Water” with an accuracy of 99 % (Table 4.5.). Visual display of accuracy assessment representing classification ambiguity of segments can also be seen in Figure 4.11.

Table 4.4: Features extracted from randomly selected sample segment representing ranges for membership boundaries of subset image sample scene for Case 2.

FEATURES	Membership Boundaries		
	Oil Slick	Look-alike	Clear Sea Water
Mean Layer Value (8-bit Morph.)	62-78	65-92	125 - 160
Mean Layer Value (Lee-Frost-Kuan)	565-580	555-600	670 – 745
Brightness	305-330	310-347	345 – 450
Min. Pixel Value (8-bit Morph.)	11-24	8-20	35 – 68
Max. Pixel Value (8-bit Morph.)	105-129	113-143	175 – 225
Mean difference to Neighbor Pixels	(-50) - (-33)	(-20) - 1	(-7) – (-1)
Mean difference to Scene	(-95) - (-71)	(-93) - (-51)	25 – 90
Area (meter square)	300 - 2300	500 - 1900	300 – 1400
Length / Width	2,7 – 5,8	1 – 1,5	1,4 – 1,8
Compactness	2,4 – 4,7	1,7 – 2,3	2 – 3
Shape Index	2,8 – 5,0	1,8 – 2,5	2,2 - 2,7
Homogeneity	0,033-0,047	0,040-0,047	0,043 – 0,048
Contrast	930-1172	900-1070	780 – 900
Dissimilarity	22-27	22-25	21 – 23

Table 4.5: Results of Accuracy Assessment for subset image sample scene for Case 2.

	Classification Stability				
CLASS	**Objects**	**Mean**	**Std. Dev.**	**Min.**	**Max.**
Probable Oil Slick	38	0,6579	0,4744	0	1
Probable Look-alike	420	0,7929	0,4053	0	1
Clear Sea Water	6436	0,9900	0,0841	0	1

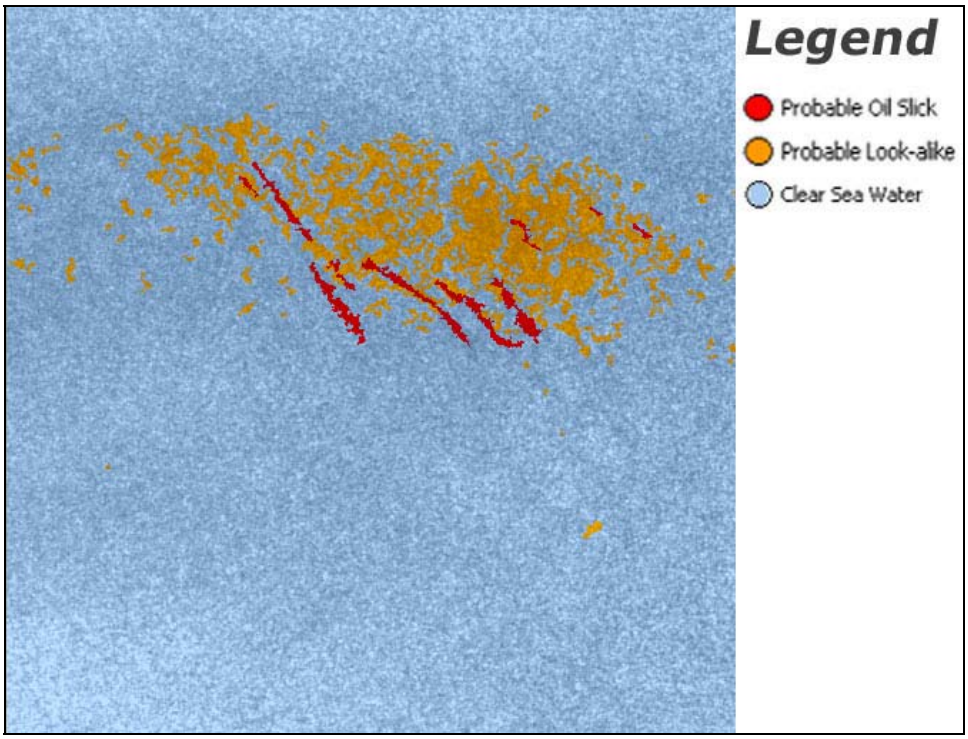

Figure 4.10: Classified subset image sample scene for Case 2 representing the discrimination of two dark spot classes.

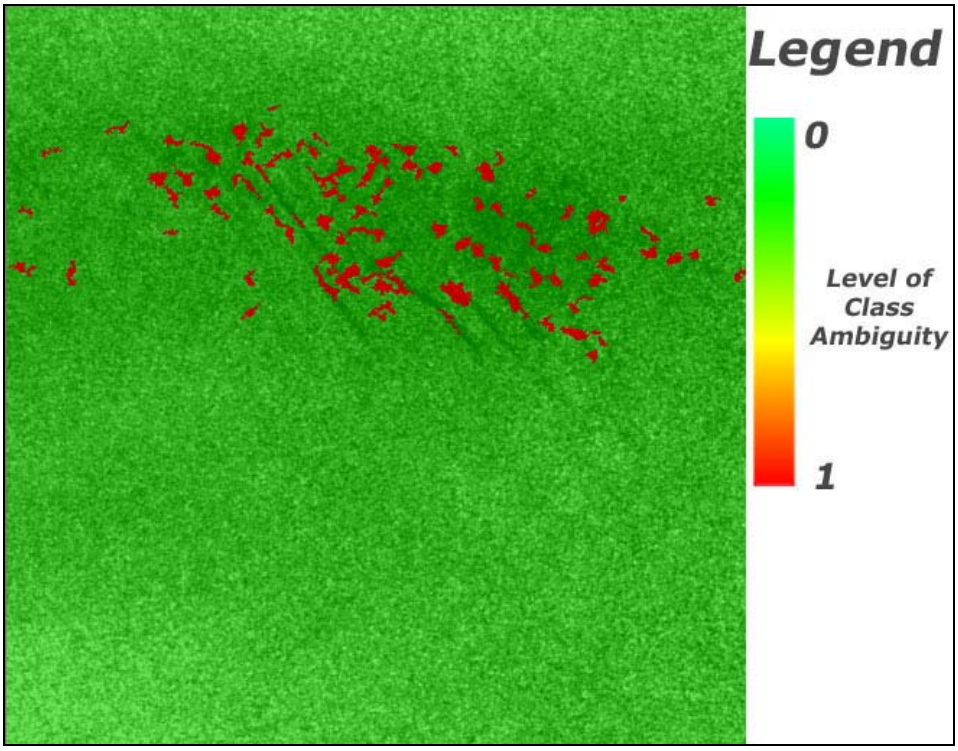

Figure 4.11: Visual Display of Class Stability Accuracy Assessment for subset image sample scene for Case 2.

4.2.3. Case 3

The third case is contains dark spots isolated from the surroundings in homogeneity, contrast and shape. The same steps as in the previous cases have been followed for segmentation process and input data sets have been prepared (Figure 4.12).

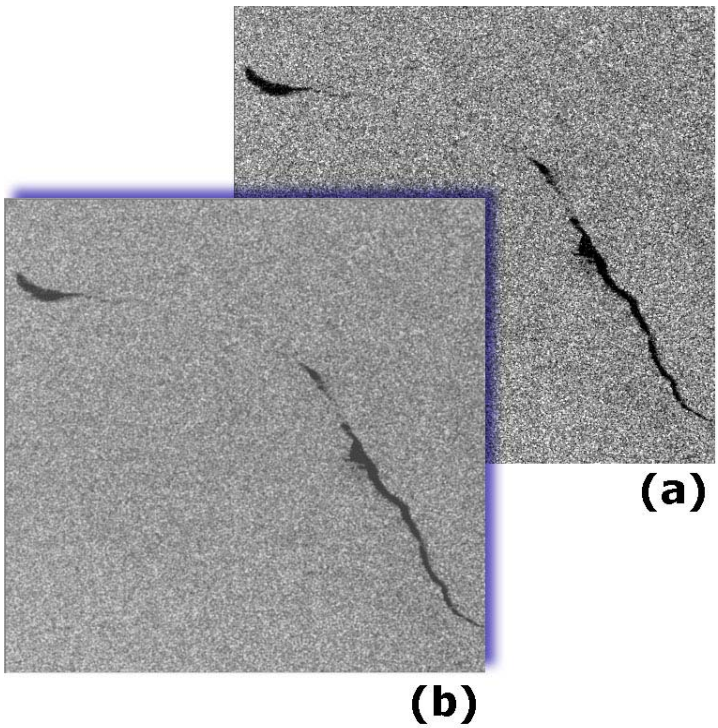

Figure 4.12: (a) Successive speckle filter subset image sample scene for Case 3, (b) Opening morphology filter applied subset image sample scene for Case 3.

The difference of this case from previous cases is the abruptness of dark spot areas from the rest of the scene. Three different levels of segmentation have been applied to the input images and it has been observed that increment in the scale factor provided identification of dark spots with single segments rather than multiple segments (Figure 4.13). Smaller and more representative segments have been created for dark spots whereas larger and more heterogeneous segments have been created for lighter regions, which shadow dark spot information with small scale. This different level of segmentation is another approach in object based

classification and these three levels of segments have been used in feature extraction stage. The classification has been made based on smaller scale parameter which is 20 and the other segmentation parameters kept the same as the previous cases. In this Case, dominant features directing the classification are 'Mean difference to Neighbor Pixels', 'Mean difference to Scene', 'Minimum Pixel value', Brightness, Homogeneity, and Contrast (Table 4.6).

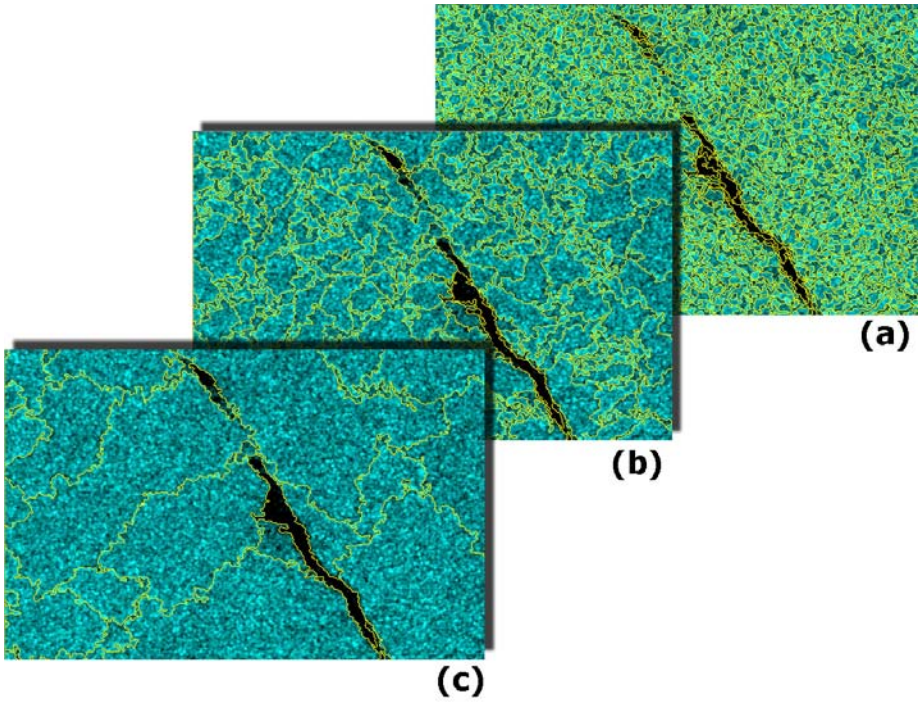

Figure 4.13: Segmented subset image sample scene for Case 3 (a) Scale Parameter 20, (b) Scale Parameter 50, (c) Scale Parameter 100.

While defining the membership functions for discrimination of dark spot subclasses classification process shows a small variation. Randomly selected sample segments for "Probable Look-alike" class have not been found to be representative since both the segments are so small and the samples are ambiguous. For that reason, dark spot class has been defined by membership functions obtained from 'Minimum Pixel value' and 'Brightness', "Probable Oil Slick" has been defined by membership functions obtained from

'Mean difference to Scene', 'Homogeneity', and 'Contrast' and "Probable Look-alike" class has been defined with a "not" logical operator containing dark spot segments which are not belonging to "Probable Oil Slick" class (Figure 4.14). In The result of 'Classification Stability' showed that, 67 segments out of 7601 have been classified as "Probable Oil Slicks" with an accuracy of 94 %, 28 segments have been classifies as "Probable look-alikes" with an accuracy of 57 %, and 7506 segments have been classified as "Clear Sea Water" with an accuracy of 99 % (Table 4.7). The classification accuracy has also been represented visually in terms of ambiguity levels in Figure 4.15 and it can be observed that most of the ambiguous segments are belonging to "Probable look-alikes" class.

Table 4.6: Features extracted from randomly selected sample segment representing ranges for membership boundaries of subset image sample scene for Case 3.

FEATURES	Membership Boundaries		
	Oil Slick	Look-alike	Clear Sea Water
Mean Layer Value (8-bit Morph.)	60-85	70-95	140 - 165
Mean Layer Value (Lee-Frost-Kuan)	346-388	380-500	490 – 560
Brightness	205-235	230-310	315 – 370
Min. Pixel Value (8-bit Morph.)	28-54	35-70	85 – 135
Max. Pixel Value (8-bit Morph.)	92-119	105-143	170 – 225
Mean difference to Neighbor Pixels	(-61) - (-22)	(-20) - 10	(-34) – 39
Mean difference to Scene	(-169) - (-143)	(-95) - (-49)	(-24) – 41
Area (meter square)	265 - 1171	300 - 560	450 – 900
Length / Width	1,1 – 3,7	1,2 – 2,7	1,1 – 2,1
Compactness	2,1 – 2,4	1,5 – 2,5	1,7 – 2,6
Shape Index	1,9 – 2,8	1,6 – 2,4	1,6 – 3,1
Homogeneity	0,024-0,040	0,038-0,042	0,026 – 0,036
Contrast	1324-2140	1230-1690	1160 – 1820
Dissimilarity	25-35	23-27	25 – 33

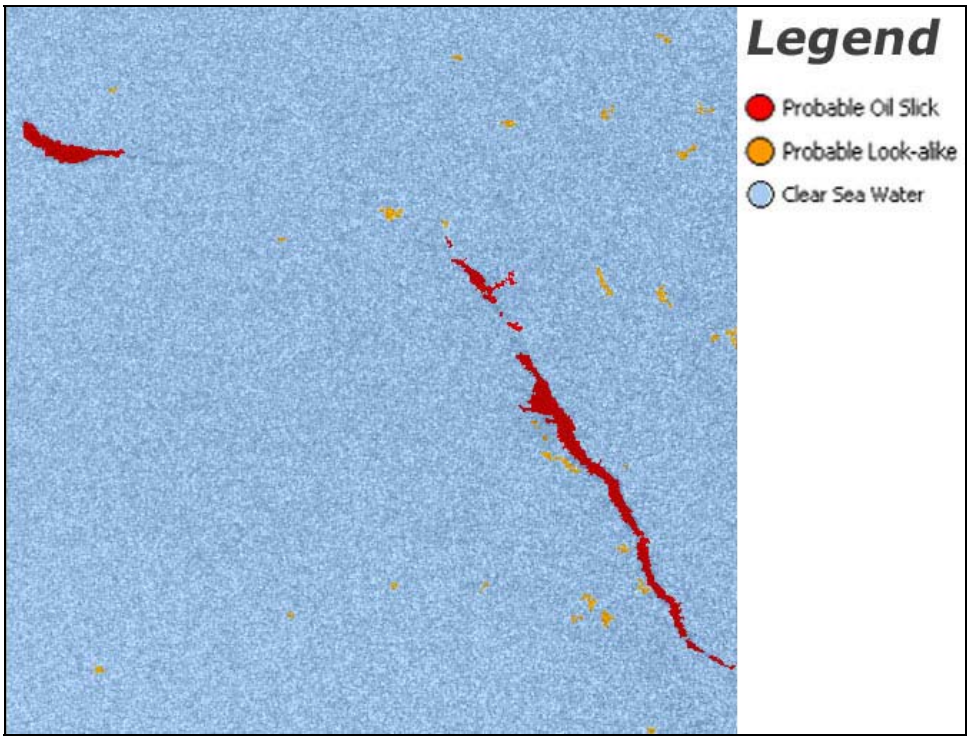

Figure 4.14: Classified subset image sample scene for Case 3 representing the discrimination of two dark spot classes.

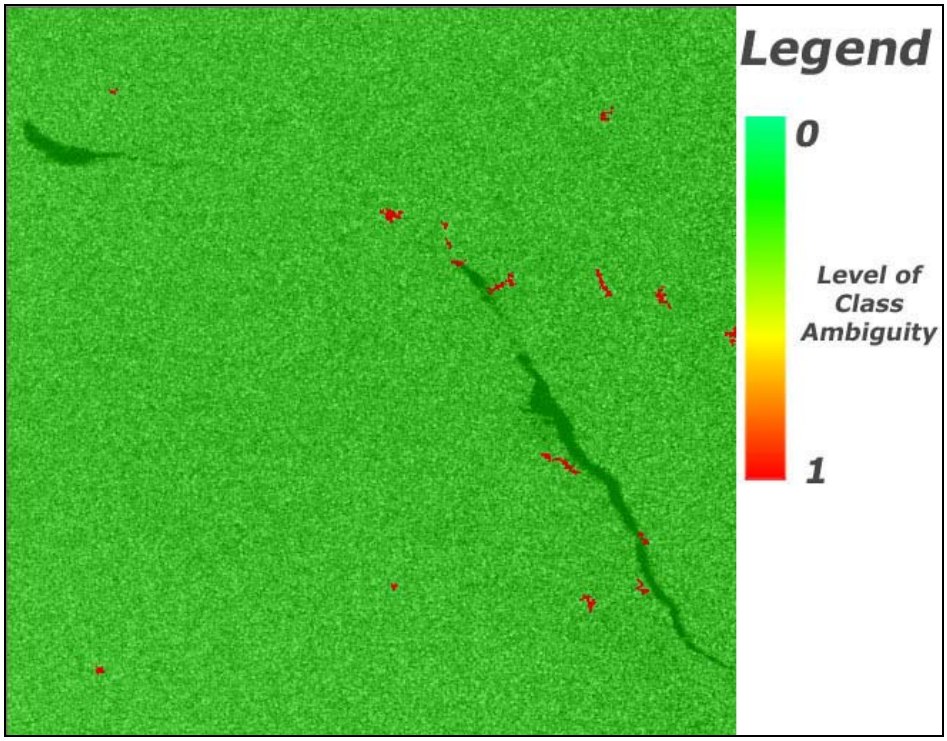

Figure 4.15: Visual Display of Class Stability Accuracy Assessment for subset image sample scene for Case 3.

Table 4.7: Results of Accuracy Assessment for subset image sample scene for Case 3.

	Classification Stability				
CLASS	**Objects**	**Mean**	**Std. Dev.**	**Min.**	**Max.**
Probable Oil Slick	67	0,9403	0,2369	0	1
Probable Look-alike	28	0,5714	0,4949	0	1
Clear Sea Water	7506	0,9950	0,0751	0	1

CHAPTER 5

DISCUSSIONS

Most of the well known conventional image classification techniques are multi/hyperspectral and either pixel based or parcel based. However, SAR data is single band and only parameter that can be taken into account is the digital number value of pixels. Even if pixel based classification techniques are applied the results would not be more representative than the results of speckle and morphology filters. As these filters already constitutes the pixel based part of the proposed classification method. Furthermore, pixel thresholding can also detect the dark areas from the lighter surroundings, but discrimination of look-alikes and oil slicks is not possible. Every single pixel having lower pixel value than the threshold is going to be defined as an oil slick, which might lead to erroneous results. In the proposed methodology, the strongest point is combination of pixel based filtering, supervision of human interpreter, object based segmentation and fuzzy classification. In object based classification the pixels are groups to segments based on the two different input data. More over input data provided good background for the extracted features. Membership functions helped to adjust the specific character of every individual subset. The membership functions work as kind of thresholding and binarization of individual segments. The algorithm converts every segment to a binary object with the help of Boolean range membership function. The segments having the value of “1” for every membership function tied with ‘and’ logical operator are assigned to one specific class.

As it is mentioned in the previous section the subsets are categorized into three cases. Every individual scene has its own feature character and the membership boundaries should be reevaluated. In every case the weight or the impact of each extracted feature is not the same. For the first case, which has moderate contrast difference with the surroundings, features related to layer values and texture found to be more determinative than the

shape related features. Shape related features are important when the segment totally represents the dark spot area. They proved their importance in second case, which has low contrast difference with the surroundings. Shape index, Compactness and Length to Width Ratio features were found to be representative than the texture features. Area features directly related to size of the segments and therefore to the scale parameter. Increasing the scale parameter increases the segment area and segments containing the whole dark spot can be classified using area values. However, in most of the cases the dark spots are represented by multiple segments thus, the impact of area feature has been found to be the least. Texture feature like contrast homogeneity and dissimilarity together with layer feature of 'mean difference to scene' was the dominating features in class definitions of third case which has high contrast difference with the surroundings. Consequently, for the impact weight of the feature it can be said that layer values and texture values were more determinative for case 1 and case 3 whereas, layer values and shape values was more discriminative in case 2.

One other aspect of discussion is the accuracy assessment which is the most important part of an image classification. The classification accuracy has been calculated from class stability and best classification results, in which shows the basic statistics and probability of segments belonging to the classes that they are assigned by the fuzzy logic defined by the membership functions. Since there is neither training set for class definition nor control set for accuracy assessment, consistency of classes within themselves can be measured. However, it should be kept in mind that, there is always a risk of obtaining wrong results even if class stability results show high level of consistency. Overall classification accuracy has been calculated as averaging the results obtained from three cases. An average classification accuracy of 83 % for "Probable Oil Slicks", 77 % for "Probable look-alikes" and 98.6 % for "Clear Sea Water" classes has been calculated. In order to focus on the main scope of the method it has been observed that the accuracy of classifying "Probable Oil Slicks" decreases when the contrast difference of dark spots with the surroundings decreases. Case 2 is a good example of this situation. Conversely, classification accuracy of "Probable look-alikes" class decreases when contrast difference heterogeneity of the scene increases. Case 3 can be shown as an example of this situation.

One of the weakest point of the classification method is determination of the origin of the slicks in other words, the discrimination of man made oil spills and the natural slicks. There is always a probability of classified oil slicks to be originated from man made structures like petrol platforms or ships. These features appear as very bright spots in size of few pixels and the dark spots in the near neighborhood can be in relation with them. Since there is not any known offshore oil platform in the region the most common sources for man made spills are the commercial ships. Major ship track ways can be used to optimize the false alarms for naturally originated slicks. However, in place of this information, temporal continuity can be checked and it is more efficient in determining the source of the oil on the sea surface. If the oil is coming from a definite source at sea bottom dark spots should be consistently present in a near neighborhood of pre-existing dark spot at different times. Location, orientation, and texture can be different from scene to scene based on the atmospheric conditions, weathering effect on the sea surface, and disruption within the water column. Throughout the 20 scenes of 3 different dates obtained from 16 subsets 75 % showed repetition in more than one image. It is known from literature that the optimal wind speed to observe exact shape and pattern of slicks is between 3 and 10 m/s. Wind speeds lower than 3 m/s oil becomes inseparable from smooth sea surface and in higher wind speeds slicks also can not be observed because of high rate of weathering and dispersion. Even more, slicks can not be present in the scene depending on the time of image accusation and the incoming flux rate. Because of the special condition of Black Sea it is very common to have this situation.

One of the latest researches for offshore hydrocarbon seepage in Central Black Sea region around Andrusov High was “Koca Piri Reis” Excursion Cruise which was completed in November 2005 in corporation of Turkish Petroleum Company, 9 Eylül University, and Middle East Technical University. During that research several oil and gas seep locations has been discovered. One of them was a mud volcano named as “Piri Reis” located at offshore Sinop, South Eastern part of Andrusov High. The significance of that survey was to be one of the early attempts for utilization of satellite SAR imagery for the region. Some of the seismic lines were arranged based on the former information extracted from SAR imagery. Rather than SAR imagery and 2-D seismic applications, gravity core sampling for the target

areas of hydrocarbon seepage and ground verification oil slicks detected by SAR imagery have been conducted.

To sum up, when all the background information and the results of the classification are taken into consideration, it can be said that the proposed classification method is sufficient enough to discriminate oil slicks from look-alikes. Method includes human supervision as well as automated algorithms in all of the levels, which is also another factor to increase the accuracy and reliability of the classification. During the image processing and classification stages small subset of 1024 x 1024 pixel size has been used in order to reduce the time for computer processing stage. Larger size of images can also be filtered and classified with the proposed methodology by the help of more powerful computer systems. Oil slick phenomenon is a fuzzy subject and required plenty of background knowledge. The weakest point is in the temporal aspect concerning separation of spills and slicks. This weakness can be improved by increasing number of images from different dates. Even though there are more images from different dates they should be classified separately and interpreted together with the seismic sections for the same location in order to relate sea surface with the subsurface geology and give the best explanation about the origin of the slicks.

CHAPTER 6

CONCLUSIONS

In this study we aimed to develop a method for offshore oil slick detection using satellite remote sensing. Since offshore petroleum exploration highly multidisciplinary subject, various background information has been presented. When all the background information, including hydrocarbon seep, oil slicks, remote sensing techniques, regional, atmospheric, and geological properties of Black Sea, have been taken into consideration, it can be said that, most of the objectives of this research have been achieved. The major conclusion of the study is; proposed satellite remote sensing technique and classification methodology, composed of visual inspection, image filtering, and object based fuzzy classification, using satellite Synthetic Aperture Radar (SAR) image manifested good results for detection and classification of offshore oil slicks.

In the thesis, an adapted system for detection of oil slicks in ENVISAT images has been presented. Major part of the oil slick detection problem was to distinguish oil slicks from other natural phenomena that create dark patches in the SAR image. The detection approach was divided into 3 levels; two for dark spot detection and one for dark spot classification. Detection Stage was including visual interpretation and automated image filtering. Classification level was composed of segmentation, feature extraction and object based fuzzy classification. The object based classification method was a kind of supervised approach used to reduce the number of false alarms based on the slick feature extraction describing layer values, shape, and texture.

The methodology worked satisfactorily in different oil slick detection cases resulting three main advantages. First, the effect of sea state conditions is optimized. This is achieved by the speckle and the morphology filters. Second, false classification due to pixel based approach has been removed with the object based approach and further discrimination between

oil slicks and look-alikes became applicable. Third, the method is semi automated, in other words it is both in control of an automated classification system and human interpreter yielding a more reliable knowledge base classification.

The accuracy of classification was different for different cases of dark spots. For the first case, which has multiple orientation and moderate level of contrast to the surroundings, the accuracy was 90 %, 95 %, and 98 % for “Probable Oil Slicks”, “Probable look-alikes”, and Clear Sea Water” classes respectively. For the second case, which has unique orientation and low level of contrast, the accuracy was 65 %, 79 %, and 99 % for “Probable Oil Slicks”, “Probable look-alikes”, and Clear Sea Water” classes respectively. For the third case, which has unique orientation and high level of contrast to the surroundings, the accuracy was 94 %, 57 %, and 99 % for “Probable Oil Slicks”, “Probable look-alikes”, and Clear Sea Water” classes respectively. The overall accuracy obtained by averaging three different cases is 83 % for oil slicks and 77 % for look-alikes. In literature for similar studies from different researchers, the accuracy may be even better but comparison of accuracy of methods cannot provide reliable conclusions because different data set and different research area. The main disadvantage of the method developed was the limited number of data sets and lack of information about atmospheric data.

For offshore hydrocarbon seepage exploration the presented methodology can be considered to be a preliminary work and interesting supplementary information can be extracted for determining the best operational procedure. However, aircraft or ship cruises are still needed for oil slick verification. As a result of study it is observed that adopted and modified methodology is very effective in dark spot detection and classification. However, it needs improvement in the aspects of discrimination of natural slicks from man made spills. That improvement can be achieved by using many other data sets from different dates, wind information of the field, expert knowledge of source of seeps. Further recommendations for research on this issue includes validation of classified oil slicks on more images in the same location with various sea states. A database of the slicks for temporal concerns should be constructed to monitor the dark spots caused by natural seeps. Major track ways of ship cruises or any other stable source of pollution should be identified.

Continuous monitoring is necessary because hydrocarbon seeps are stable, therefore oil slicks should also be stable. Of course the location an orientation will not be identical in every image because of atmospheric conditions. Three sets of SAR images were present for research area which also gave significant clues about temporal continuity however; continuous monitoring with several other sets of images will increase the reliability of the results.

REFERENCES

Abrams, M. A. 2005, Significance of hydrocarbon seepage relative to petroleum generation and entrapment, Marine and Petroleum Geology Vol. 22, pp. 457–477.

Allan, T.D. 1983, Satellite microwave remote sensing, Chichester, West Sussex: E. Horwood ; New York. 526 pages.

Almeida-Filho, R., de Miranda, F.P., Lorenzzetti, J.A., Pedroso, E.C., Beisl, C.H., Landau, L., Baptista, M.C., Camargo, E.G. 2004, Exploration assessment in a petroleum frontier area offshore the Amazon River mouth using RADARSAT-1 images, Geoscience and Remote Sensing Symposium, IGARSS '04. Proceedings. 2004 IEEE International Vol. 6, pp. 4135 – 4138.

Almeida-Filho, R., Mıranda, F. P., Yamakawa, T. 1999, Remote detection of a tonal anomaly in an area of hydrocarbon microseepage, Tucano basin, north-eastern Brazil, International Journal of Remote sensing, Vol. 20 No. 13, pp. 2683–2688.

Arvelyna Y., Oshima, M., Kristijuno, A., Gunawan, I. 2001, Auto Segmentation of oil slick in RADARSAT SAR Image Data Around Rupat Island, Malaca Strait, 22nd Asian Conference on Remote Sensing.

Bakan, G. and Büyükgüngör, H. 2000, The Black Sea, Marine Pollution Bulletin, Vol. 41, No. 1-6, pp. 24-43.

Bertacca, M., Berizzi, F., Mese,E. D. 2005, A FARIMA-Based Technique for Oil Slick and Low-Wind Areas Discrimination in Sea SAR Imagery, IEEE Transactıons On Geoscıence And Remote Sensıng, Vol. 43, No. 11, pp.2484-2493.

Brekke C., Solberg A. H.S. 2005, Oil spill detection by satellite remote sensing, Remote Sensing of Environment, Vol. 95, pp. 1–13.

Clarke, R. H., Cleverly, R. W. 1991, Petroleum seepage and post-accumulation migration. In: England WA, Fleet JA (Eds) Petroleum migration. Geological Society Publication, Geological Society Publication, pp. 265–271.

Daling, P. S., StrØm, T. 1999, Weathering of Oils at Sea: Model/Field Data Comparisons, Spill Science & Technology Bulletin, Vol. 5, No. 1, pp. 63-74.

Del Frate, F., Petrocchi, A., Lichtenegger, J., Calabresi, G. 2000, Neural Networks for Oil Spill Detection Using ERSSAR Data, *IEEE Trans. Geosci. and Remote Sensing*, Vol. 38, pp. 2282-2287.

eCognition, 2004, User Guide, Definiens Imaging GmbH, München, Germany, 486 pages.

ESA, European Space Agency. 2004, ENVISAT-ASAR product handbook.

Espedal, H. 1999, Detection of oil spill and natural film in the marine environment by spaceborne SAR. Proc. IGARSS'99, Vol. 3, pp. 1478 – 1480.

Espedal, H. A., Johannessen, O. M. 2000, Detection of oil spills near offshore installations using synthetic aperture radar (SAR). International Journal of Remote Sensing, Vol. 21, No. 11, pp. 2141–2144.

Espedal, H. A., Wahl, T. 1999, Satellite SAR oil spill detection using wind history information. International Journal of Remote Sensing, 20(1), 49–65.
MacDonald I.R., Leifer I., Sassen P., Stine P.,Mitchell R., and Guinasso J.R. 2002, Transfer of Hydrocarbons From Natural Seeps to the Water Column and Atmosphere, Geofluids, Vol. 2, pp. 95-107.

Ergün M., Dondurur D., Çifçi G.. 2002, Acoustic evidence for shallow gas accumulations in the sediments of the Eastern Black Sea, Terra Nova, Vol. 14 No:5, pp. 313-320.

Fingas, M. F., Brown, C. E. 1997, Review of oil spill remote sensing. Spill Science and Technology Bulletin, Vol. 4, No.4, pp. 199–208.

Fiscella, B., Giancaspro, A., Nirchio, F., Pavese, P., & Trivero, P. 2000. Oil spill detection using marine SAR images. International Journal of Remote Sensing, Vol. 21, No. 18, pp. 3561–3566.

Friedman, K.S., Pichel, W.G., Clemente-Colon, P., Xiaofeng Li. 2002, International Geoscience and Remote Sensing Symposium,. IGARSS '02 Vol. 6, pp. 3343–3345.

Frost, V.S., Stilles, J.A., Shanmugan, K.S., and Holtsman, J.C. 1982, A model for radar images and its application to adaptive digital filtering of multiplicative noise, IEEE Trans. Pattern analysis and Machine Intelligence Vol.4 Issue 2 pp. 157-166.

Girard-Ardhuin F, Mercier G, Collard F, et al. 2005, Operational oil-slick characterization by SAR imagery and synergistic data, IEEE Journal Of Oceanıc Engıneerıng, Vol. 30, No. 3, pp. 487-495.

Girard-Ardhuin, F., Mercier, G., Garello, R. 2003, Oil slick detection by SAR imagery: potential and limitation. Proc. OCEANS 2003, Vol. 1, pp. 164–169.

Gonzalez, R. C., Richard E. W. 1992, Digital Image Processing, Addison-Wesley Publishing Co, 716 pages.

Greinert J., Artemov Y., Egorov V., De Batist M., McGinnis D. 2006, 1300-m-high rising bubbles from mud volcanoes at 2080m in the Black Sea: Hydroacoustic characteristics and temporal variability, Earth and Planetary Science Letters, Vol. 244, pp. 1–15.

Haralick, R. M. 1979, Statistical and Structural Approaches to Texture, Proceedings of the IEEE, Vol. 67, No. 5, pp. 786-804.

Haralick, R. M., Shanmugan, K, Dinstein, I. 1973, Textural Features for Image Classification, IEEE Tr. on Systems, Man and Cybernetics, Vol SMC-3, No. 6, pp. 610-621.

Hofmann, T., Puzicha, J., Buhmann, J. 1998, Unsupervised texture segmentation in a deterministic annealing framework. In: IEEE Transactions on Pattern Analysis and Machine Intelligence. Vol. 20, No. 8, pp. 803-818.

Hovland, H. A., Johannessen, J. A., Digranes, G. 1994, Slick detection in SAR images. Proc. IGARSS'94, Vol. 4, pp. 2038–2040.

Huang, B, Li, H, Huang, X 2005, A level set method for oil slick segmentation in SAR images, International Journal of Remote Sensing, Vol. 26, No. 6, pp. 1145–1156.

Karathanassi, V., Topouzelis, K., Pavlakis, P., And Rokos, D. 2006, An object-oriented methodology to detect oil spills, International Journal of Remote Sensing Vol. 27, No. 23, pp. 5235–5251

Keramitsoglou, I., Cartalis, C., Kiranoudis, C. T. 2006, Automatic identification of oil spills on satellite images, Environmental Modelling & Software, Vol. 21, pp. 640–652.

Kruglyakova, R., Gubanov, Y., Kruglyakov, V., Prokoptsev G. 2002, Assessment of technogenic and natural hydrocarbon supply into the Black Sea and seabed sediments, Continental Shelf Research Vol. 22, pp. 2395–2407.

Kuan, Sawchuck, A.A., Strand, T.C., and Chavel, P. 1985, Adaptive restoration of images with speckle, IEEE Trans. ASSP, Vol. 35, No. 3, pp. 373-383.

Lee, Jong-Sen. 1980, Digital Image Enhancement and Noise Filtering by Use of Local Statistics, IEEE Transactions on Pattern Analysis and Machine Intelligence, Vol. PAMI-2, No.2, pp. 165-168.

Leifer, I., Luyendyk, B., Broderick, K. 2006, Tracking an oil slick from multiple natural sources, Coal Oil Point, California, Marine and Petroleum Geology Vol. 23, pp. 621–630.

Lennon, M.; Thomas, N., Mariette, V., Babichenko, S., Mercier, G. 2005, Oil slick detection and characterization by satellite and airborne sensors: experimental results with SAR, hyperspectral and lidar data, Geoscience and Remote Sensing Symposium, IGARSS '05. Proceedings. 2005 IEEE International, Vol. 1, pp. 1-4.

Lombardo P., Oliver, C.J. 2000, Optimum detection and segmentation of oil-slicks using polarimetric SAR data, IEE Proc.-Radar, Sonar Navigation., Vol. 147, No. 6, pp.309-321.

Lu, J. 2003, Marine oil spill detection, statistics and mapping with ERS SAR imagery in south-east Asia, International Journal of Remote Sensing, Vol. 24, No. 15, pp. 3013–3032.

Mao, J., Jain A. 1992, Texture classification and segmentation using multiresolution simultaneous autoregressive models, In: Pattern Recognition, Vol. 25, pp. 173-188.

Marghany, M. 2001, RADARSAT automatic algorithms for detecting coastal oil spill pollution, JAG, Vol. 3, No. 2, pp. 191-196.

Marghany, M. 2004, RADARSAT for oil spill trajectory model, Environmental Modelling & Software Vol. 19, pp. 473–483.

Mazzini A., Ivanovb M.K., Parnella J., Stadnitskaia A., Cronin B.T., Poludetkina E., Mazurenko L.,Van Weering T.C.E. 2004, *Methane-related authigenic carbonates from the Black Sea:geochemical characterisation and relation to seeping fluids*, Marine Geology, Vol. 212, pp. 153–181.

Mouche A.A., Hauser D., Daloze J., and Guérin C. 2005, Dual-Polarization Measurements at C-Band Over the Ocean: Results From Airborne Radar Observations and Comparison With ENVISAT ASAR Data, IEEE Transactıons On Geoscıence And Remote Sensıng, Vol. 43, No. 4.

Nikishin A.M., Korotaev M. V., Ershov A. V., Brunet M. 2003, The Black Sea basin: tectonic history and Neogene–Quaternary rapid subsidence modelling, Sedimentary Geology, Vol. 156, pp. 149–168.

Nirchio F., Sorgente M., Giancaspro A., Biamino W., Parisato E., Ravera R., and Trivero P. 2005. Automatic detection of oil spills from SAR images, International Journal of Remote Sensing Vol. 26, No. 6, pp.1157–1174.

O'Brien, G. W., Lawrenceb, G. M., Williamsc, A. K., Glennd, K., Barrettd, A.G., Lechd, M., Edwardsd, D. S., Cowleye, R., Borehamd, C. J., Summonsf, R. E. 2005, Yampi Shelf, Browse Basin, North-West Shelf, Australia: a test-bed for constraining hydrocarbon migration and seepage rates using combinations of 2D and 3D seismic data and multiple, independent remote sensing technologies, Marine and Petroleum Geology, Vol. 22, pp: 517–549.

Okay, A.I., Celal Sengor, A. M. C., and Gorur, N. 1994 Kinematic history of the opening of the Black Sea and its effect on the surrounding regions, *Geology*, Vol. 22, No. 3, pp. 267-270

Özhan, E., Abdalla, S. 2002, Türkiye Kıyıları Rüzgar ve Derin Dalga Atlası, Kıyı Alanları Yönetimi Türk Milli Komitesi / MEDCOAST, Orta Doğu Teknik Üniversitesi, 405 sayfa (in Turkish)

Pellemans, A.H.J.M., Bos, W.G., Konings, H., van Swol, R.W. 1995, Oil Spill Detection on the North Sea using ERS-1 SAR Data, Beleids Commisie Remote Sensing, BCRS report 94-30.

Roberts, D. G. 1998, Regional and Petroleum Geology of the Black Sea and Surrounding Region, Marine and Petroleum Geology, Vol. 15, No. 4, pp. 381-383.

Robinson A.G., Rudat J.H., Banks C.J., Wiles R.L.F. 1996, *Petroleum geology of the Black Sea,* Marıne and Petroleum Geology, Vol.13, No. 2, pp. 195-223.

Rollet, N., Logan, G. A., Kennard, J. M., O'Brien, P. E., Jones, A. T., Sexton M. 2006, Characterisation and correlation of active hydrocarbon seepage using geophysical data sets: An example from the tropical,carbonate Yampi Shelf, Northwest Australia, Marine and Petroleum Geology, Vol. 23, pp. 145–164.

Russ, J. C. 1992, The Image Processing Handbook, CRC Press, 445 pages.

Ryerson, R. A. 1998, Manual of remote sensing: Imaging Radar, American Society for Photogrammetry and Remote Sensing, J. Wiley, vol. 2.

Sabins, F. F., 1997, Remote Sensing: Principles and Interpretation, 3rd edn (New York: W. H. Freeman).

Smith, A. J. E., Melger, F. J. 2003, Using the cross-spectral phase to filter slicks in the ENVISAT ASAR wave mode product, International Journal of Remote sensing, Vol. 24, No. 24, pp. 5391–5396.

Solberg, A. H. S., Brekke, C., Husøy P. O. 2007, Oil Spill Detection in Radarsat and Envisat SAR Images, IEEE Transactions On Geoscience And Remote Sensing, Vol. 45, No. 3, pp: 746-755.

Solberg, A. H. S., Dokken, S. T., & Solberg, R. 2003. Automatic detection of oil spills in Envisat, Radarsat and ERS SAR images. Proc. IGARSS'03, Vol. 4, pp. 2747–2749.

Solberg, A. H. S., Storvik, G., Solberg, R., & Volden, E. 1999, *Automatic detection of oil spills in ERS SAR images*. IEEE Transactions on Geoscience and Remote Sensing, Vol. 37, No. 4, pp. 1916–1924.

Solberg, A. H. S., Volden, E. 1997, Incorporation of prior knowledge in automatic classification of oil spills in ERS SAR images. Proc. IGARSS'97, Vol. 1, pp. 157–159.

Staneva, J.V., Dietrich, D. E., Stanev, E. V., Bowman, M. J. 2001, Rim current and coastal eddy mechanisms in an eddy-resolving Black Sea general circulation model, Journal of Marine Systems, Vol. 31, pp. 137–157.

Struckmeyer, H.I.M., Williams, A.K., Cowley, R., Totterdel, J.M., Lawrance, G., O'Brein G. W. 2002, Evaluation of hydrocarbon seepage in the great Australian Bigth, APEA Journal, pp.371-385.

T.P.A.O., Turkish Petroleum Company. Özçelik, Y., Öner, A. F., Özbek, G., Demirer, A. and others. 1997, The TPAO/BP Eastern Black Sea Concession Area Evaluation Report, No. 3970, 301 pages.

TNTmips, 2001, User Manual, "Getting Started", Microimages, Lincoln, NE, USA, 1065 pages.

The International Tanker Owners Pollution Federation Limited (ITOPF), 2002. Tecnical Information Paper: Fate of Marine Oil Spills, No. 2, 8 pages

Van der Meer, F., Van Dijk, P., Van der Werff, H., Yanga, H. 2002, Remote sensing and petroleum seepage: a review and case study, Terra Nova, Vol. 14, No. 1–17, pp.1-17.

Woodhouse, I. H. 2006, Introduction to microwave remote sensing, Taylor & Francis, 370 pages.